Relativistic numerical models for stationary superfluid Neutron Stars

Reinhard Prix
Max-Planck-Institut für Gravitationsphysik, Albert-Einstein-Institut, Am Mühlenberg 1, D-14476 Golm, Germany

Jérôme Novak
Laboratoire de l'Univers et de ses Théories, Observatoire de Paris, F-92195 Meudon Cedex, France

G. L. Comer
Department of Physics, Saint Louis University, St. Louis, MO, 63156-0907, USA
(Dated: Jan 24, 2005)

We have developed a theoretical model and a numerical code for stationary rotating superfluid neutron stars in full general relativity. The underlying two-fluid model is based on Carter's covariant multi-fluid hydrodynamic formalism. The two fluids, representing the superfluid neutrons on one hand, and the protons and electrons on the other, are restricted to uniform rotation around a common axis, but are allowed to have different rotation rates. We have performed extensive tests of the numerical code, including quantitative comparisons to previous approximative results for these models. The results presented here are the first "exact" calculations of such models in the sense that no approximations (other than that inherent in a discretized numerical treatment) are used. Using this code we reconfirm the existence of prolate-oblate shaped configurations. We studied the dependency of the Kepler rotation limit and of the mass-density relation on the relative rotation rate. We further demonstrate how one can simulate a (albeit fluid) neutron-star "crust" by letting one fluid extend further outwards than the other, which results in interesting cases where the Kepler limit is actually determined by the outermost but *slower* fluid.

I. INTRODUCTION

The aim of this work is to calculate fully relativistic stationary models of superfluid neutron stars including all non-dissipative couplings between the two fluids induced by the equation of state (EOS), in particular the entrainment effect. In addition to studying the stationary properties of relativistic superfluid neutron stars, these models can serve as the unperturbed initial state in a dynamical study of neutron star oscillations, neutron star collapse to a black hole, or as a starting point in studying pulsar glitch-models.

Neutron stars are fascinating astrophysical objects: on one hand they represent a formidable "laboratory" of fundamental physics, as the composition and equation of state of their inner core still lies beyond the reach of experimental and theoretical physics. On the other hand, the advent of increasingly sensitive gravitational wave detectors promises to open a new observational window on neutron stars, which will allow us to gain new insights into these still rather poorly understood objects. Gravitational wave astronomy could represent the first opportunity to observe neutron star oscillations, providing a new view on their inner dynamics. Considering the success of classical terrestrial seismology and asteroseismology of the sun and of main-sequence stars, one could expect this to result in substantial progress in our understanding of the dynamics and composition of neutron stars.

Additionally, observing quasi-permanent quadrupolar deformations ("mountains") on neutron stars via gravitational waves[1] will give valuable complementary information about their rotational behavior, which is currently only observable via their electromagnetic pulses.

Most theoretical studies of neutron star dynamics have relied on rather simplistic single-fluid models. In this work we attempt a more realistic description of neutron stars by taking their superfluidity into account via the use of a two-fluid model. Neutrons and protons in neutron stars are predicted to be superfluid (e.g. see [2, 3]), and this feature forms a fundamental ingredient in the current (albeit rudimentary) understanding of the glitch phenomenon observed in pulsars (e.g. see [4–6]). Due to the superfluidity and therefore lack of viscosity of the neutrons in the crust and in the outer core, they can flow freely through the other components. The remaining constituents (i.e. crust-nuclei, electrons, muons and protons) are assumed to be "locked" together on short timescales by viscosity and the magnetic field. Thereby they form another fluid, which in the following will be referred to as "protons" for simplicity. These assumptions characterize the so-called two-fluid model of neutron stars. These two fluids are strongly coupled by the strong nuclear force acting between protons and neutrons, and therefore a hydrodynamic two-fluid framework incorporating these couplings is required for their description. This framework will be presented in the next section. Recently it was pointed out that such a two-fluid system can be subject to a two-stream instability if the relative velocity

[1] Note that this search has already begun, see [1] for a discussion and first results

of the two fluids exceeds a critical velocity [7]. This could therefore be relevant in neutron stars and might be related to the glitch phenomenon[6], which provides another motivation for studying the properties of such two-fluid systems.

In this paper we study the stationary structure of such two-fluid models, in which the two fluids are restricted to uniform rotation around a common axis, but allowing for two different rotation rates. This neutron star model was first studied quantitatively by Prix [8] in the Newtonian context using a generalized Chandrasekhar-Milne slow-rotation approximation, and neglecting the direct interactions between the two fluids. Andersson and Comer [9] used Hartle's variant of the slow-rotation approximation to study this model in general relativity. Prix et al. [10] further extended the Newtonian study to fully include all (non-dissipative) couplings via entrainment and the nuclear "symmetry-energy", and they found an analytic solution for a subclass of two-fluid equations of state (which generalizes the $P \propto \rho^2$-type polytropes). More recently, Yoshida and Eriguchi [11] have devised an alternative approach in the Newtonian case, by treating only the relative rotation between the two fluids as small, while allowing for fast rotation of the neutron star as a whole. Furthermore, Comer [12] has recently used the relativistic slow-rotation approximation to study the properties of the first available fully relativistic two-fluid EOS incorporating entrainment, which was derived by Comer and Joynt [13].

Here we present a generally relativistic numerical code for solving the full two-fluid model without approximations. A preliminary progress-report on the development of this code, and some early results were presented in [14].

While our model and code allow in principle for any given two-fluid equation of state (EOS), for the sake of simplicity and a better numerical convergence we restrict ourselves in this paper to the use of a (rather general) class of two-fluid "polytropes". This choice is also motivated by the lack of a useful two-fluid neutron star equation of state in the literature, especially concerning the aspect of entrainment. Even though Comer and Joynt [13] have a fully relativistic model that includes entrainment, it has not yet been developed to the point that it will produce a tabular equation of state that could be used in our code. We expect the qualitative features of our model to be well represented by the analytic EOS used in this work.

The plan of this paper is as follows: In section II we introduce the formalism and notation of covariant two-fluid hydrodynamics. In section III we discuss the specialization to an axisymmetric and stationary system, and we introduce the $3+1$ framework for Einstein's equations. In section IV we describe the numerical procedure for solving the resulting elliptical system of equations. The tests performed on the numerical code are discussed in section V, and our numerical results are presented in section VI. A discussion of this work is given in section VII. In appendix A we derive a new analytic Newtonian slow-rotation solution, which is used for comparison to our numerical results.

II. CANONICAL TWO–FLUID HYDRODYNAMICS

The general relativistic framework for describing a coupled two-fluid system has been developed by Carter, Langlois and coworkers [15–18], based on an elegant variational principle. The same relativistic two-fluid model was used by Andersson and Comer [9] in their slow-rotation description of superfluid neutron stars.

We consider a system consisting of two fluids, namely neutrons and "protons", which we label by n and p respectively. The kinematics of the two fluids is described by the two conserved particle 4-currents $n^\alpha_{\rm n}$ and $n^\alpha_{\rm p}$, i.e.

$$\nabla_\alpha n^\alpha_{\rm n} = 0\,, \quad \text{and} \quad \nabla_\alpha n^\alpha_{\rm p} = 0\,. \tag{1}$$

The dynamics of the system is governed by a Lagrangian density of the form $\Lambda(n^\alpha_{\rm n}, n^\alpha_{\rm p})$. Due to the requirement of covariance, the scalar density Λ can only depend on scalars, and we can form exactly three independent scalar combinations out of n^α_n and $n^\alpha_{\rm p}$, for example

$$\begin{aligned} n_{\rm n}^2 &\equiv -\frac{1}{c^2} g_{\alpha\beta} n^\alpha_{\rm n} n^\beta_{\rm n}\,, \\ n_{\rm p}^2 &\equiv -\frac{1}{c^2} g_{\alpha\beta} n^\alpha_{\rm p} n^\beta_{\rm p}\,, \\ x^2 &\equiv -\frac{1}{c^2} g_{\alpha\beta} n^\alpha_{\rm n} n^\beta_{\rm p}\,, \end{aligned} \tag{2}$$

where $g_{\alpha\beta}$ is the spacetime metric, so the Lagrangian density can be written as

$$\Lambda(n^\alpha_{\rm n}, n^\alpha_{\rm p}) = -\mathcal{E}(n^2_{\rm n}, n^2_{\rm p}, x^2)\,, \tag{3}$$

where $\mathcal{E}$ is a thermodynamic potential representing the total energy density of the two–fluid system, or "equation of state". Introducing the 4–velocities $u^\alpha_{\rm n}$, $u^\alpha_{\rm p}$ of the two fluids, which satisfy the normalization conditions

$$g_{\alpha\beta}\, u^\alpha_{\rm n}\, u^\beta_{\rm n} = -c^2\,, \quad \text{and} \quad g_{\alpha\beta}\, u^\alpha_{\rm p}\, u^\beta_{\rm p} = -c^2\,, \tag{4}$$

the particle 4–currents can be written as

$$n^\alpha_{\rm n} = n_{\rm n}\, u^\alpha_{\rm n}\,, \quad \text{and} \quad n^\alpha_{\rm p} = n_{\rm p}\, u^\alpha_{\rm p}\,, \tag{5}$$

in terms of the neutron- and proton densities $n_{\rm n}$ and $n_{\rm p}$ respectively. Variation of the Lagrangian density (3) with respect to the particle currents $n^\alpha_{\rm n}$ and $n^\alpha_{\rm p}$ defines the conjugate momenta $p^{\rm n}_\alpha$ and $p^{\rm p}_\alpha$, namely

$$d\Lambda = p^{\rm n}_\alpha\, dn^\alpha_{\rm n} + p^{\rm p}_\alpha\, dn^\alpha_{\rm p}\,. \tag{6}$$

Due to the covariance constraint (3) we can further express the conjugate momenta in terms of the currents as

$$\begin{aligned} p^{\rm n}_\alpha &= \mathcal{K}^{\rm nn}\, n_{{\rm n}\alpha} + \mathcal{K}^{\rm np}\, n_{{\rm p}\alpha}\,, \\ p^{\rm p}_\alpha &= \mathcal{K}^{\rm pn}\, n_{{\rm n}\alpha} + \mathcal{K}^{\rm pp}\, n_{{\rm p}\alpha}\,, \end{aligned} \tag{7}$$

where the symmetric "entrainment matrix" $\mathcal{K}^{XY}$ is given by the partial derivatives of $\mathcal{E}(n_{\rm n}^2, n_{\rm p}^2, x^2)$, namely[2]

$$\mathcal{K}^{\rm nn} = \frac{2}{c^2}\frac{\partial \mathcal{E}}{\partial n_{\rm n}^2}\,, \quad \mathcal{K}^{\rm pp} = \frac{2}{c^2}\frac{\partial \mathcal{E}}{\partial n_{\rm p}^2}\,, \quad \mathcal{K}^{\rm np} = \frac{1}{c^2}\frac{\partial \mathcal{E}}{\partial x^2}\,. \quad (8)$$

The equations of motion for the two fluids can be obtained from the variational principle developed by Carter [19]. In the absence of direct dissipative forces acting between the two fluids (e.g. see Langlois et al. [18]), the equations of motion will then be found as[3]

$$n_{\rm n}^\alpha \nabla_{[\alpha} p^{\rm n}_{\beta]} = 0\,, \quad \text{and} \quad n_{\rm p}^\alpha \nabla_{[\alpha} p^{\rm p}_{\beta]} = 0\,. \quad (9)$$

The energy–momentum tensor $T^{\alpha\beta}$, which is derived from the variational principle too, has the form

$$T^\alpha{}_\beta = n_{\rm n}^\alpha\, p^{\rm n}_\beta + n_{\rm p}^\alpha\, p^{\rm p}_\beta + \Psi g^\alpha_\beta\,. \quad (10)$$

If the equations of motion (1) and (9) are satisfied, the stress-energy tensor automatically satisfies $\nabla_\alpha T^{\alpha\beta} = 0$, which is a Noether-type identity of the variational principle. The generalised pressure Ψ of the two–fluid system is defined by the thermodynamical identity

$$\mathcal{E} + \Psi = -n_{\rm n}^\alpha\, p^{\rm n}_\alpha - n_{\rm p}^\alpha\, p^{\rm p}_\alpha\,, \quad (11)$$

so Ψ can be considered the Legendre-transform of the Lagrangian density Λ. Using the entrainment relation (7), we can rewrite this as

$$\frac{\mathcal{E}+\Psi}{c^2} = \mathcal{K}^{\rm nn}\, n_{\rm n}^2 + 2\mathcal{K}^{\rm np}\, x^2 + \mathcal{K}^{\rm pp}\, n_{\rm p}^2\,. \quad (12)$$

Instead of x^2 defined in (2), we will use a physically more intuitive quantity as the third independent scalar, namely the "relative speed" Δ. We define the relative speed Δ as the norm of the neutron velocity $u_{\rm n}^\alpha$ as seen in the frame of the protons $u_{\rm p}^\alpha$, or vice versa. The corresponding relative Lorentz factor Γ_Δ is therefore given by

$$\Gamma_\Delta = -\frac{1}{c^2} u_{\rm n}^\alpha u_{\rm p}^\beta\, g_{\alpha\beta} = \frac{x^2}{n_{\rm n} n_{\rm p}} = \left(1 - \frac{\Delta^2}{c^2}\right)^{-1/2}\,, \quad (13)$$

and the relative speed Δ is expressible in terms of x as

$$\Delta^2 = c^2\left[1 - \left(\frac{n_{\rm n} n_{\rm p}}{x^2}\right)^2\right]\,. \quad (14)$$

In the case of co-moving fluids (i.e. $u_{\rm n}^\alpha = u_{\rm p}^\alpha$), we see from (2) that $x^2 = n_{\rm n}\, n_{\rm p}$, and so $\Delta = 0$ as expected.

[2] The corresponding notation in Andersson and Comer [9] is $n_{\rm n}^\alpha \to n^\alpha$, $n_{\rm p}^\alpha \to p^\alpha$, $u_{\rm n}^\alpha \to u^\alpha$, $u_{\rm p}^\alpha \to v^\alpha$, $\mathcal{K}^{\rm np} \to \mathcal{A}$, $\mathcal{K}^{\rm nn} \to \mathcal{B}$, and $\mathcal{K}^{\rm pp} \to \mathcal{C}$.

[3] the square brackets denote averaged index anti-symmetrization, i.e. $2\,v_{[a,b]} = v_{ab} - v_{ba}$.

We can now equivalently consider the equation of state $\mathcal{E}$ as a function of the form $\mathcal{E}(n_{\rm n}, n_{\rm p}, \Delta^2)$, for which the first law of thermodynamics reads as

$$d\mathcal{E} = \mu^{\rm n} dn_{\rm n} + \mu^{\rm p} dn_{\rm p} + \alpha\, d\Delta^2\,, \quad (15)$$

closely analogous to the Newtonian formulation [10]. The conjugate quantities defined in this equation are the entrainment α and the neutron- and proton chemical potentials $\mu^{\rm n}$ and $\mu^{\rm p}$ (sometimes also referred to as specific enthalpies, which is equivalent in the zero-temperature case). It is often useful to characterize the entrainment by the dimensionless entrainment numbers ε_X, which we define as

$$\varepsilon_X \equiv \frac{2\alpha}{m^X n_X}\,, \quad (16)$$

where m^X is the particle rest-mass of the respective fluid, and the fluid-index is $X = {\rm n}, {\rm p}$ (no summation over X).

The conjugate variables of (15) can be expressed in terms of the kinematic scalars and the entrainment matrix $\mathcal{K}^{XY}$ as

$$\begin{aligned} \mu^{\rm n} &= \frac{c^2}{n_{\rm n}}\left(\mathcal{K}^{\rm nn} n_{\rm n}^2 + \mathcal{K}^{\rm np} x^2\right) = -u_{\rm n}^\alpha p^{\rm n}_\alpha\,, \\ \mu^{\rm p} &= \frac{c^2}{n_{\rm p}}\left(\mathcal{K}^{\rm pp} n_{\rm p}^2 + \mathcal{K}^{\rm np} x^2\right) = -u_{\rm p}^\alpha p^{\rm p}_\alpha\,, \\ \alpha &= \frac{1}{2}\mathcal{K}^{\rm np} n_{\rm n} n_{\rm p} \Gamma_\Delta^3\,. \end{aligned} \quad (17)$$

Using (14), the inverse relations can be obtained as

$$\begin{aligned} \mathcal{K}^{\rm nn} &= \frac{\mu^{\rm n}}{n_{\rm n} c^2} - \frac{2\alpha}{n_{\rm n}^2 \Gamma_\Delta^2} \\ \mathcal{K}^{\rm pp} &= \frac{\mu^{\rm p}}{n_{\rm p} c^2} - \frac{2\alpha}{n_{\rm p}^2 \Gamma_\Delta^2} \\ \mathcal{K}^{\rm np} &= \frac{2\alpha}{n_{\rm n} n_{\rm p} \Gamma_\Delta^3}\,, \end{aligned} \quad (18)$$

which reduces exactly to the corresponding relations in the Newtonian limit [10], where $\Gamma_\Delta \to 1$ and $\mu^X \to m^X c^2 + \widehat{\mu}^X$. In terms of these quantities, the generalised pressure Ψ (11) can also be written as

$$\Psi = -\mathcal{E} + n_{\rm n}\,\mu^{\rm n} + n_{\rm p}\,\mu^{\rm p}\,, \quad (19)$$

which is the generalization of the thermodynamic Gibbs-Duhem relation to a two-fluid system.

III. STATIONARY AXISYMMETRIC CONFIGURATIONS

A. The metric

Here and in the following we choose units such that $G = c = 1$ for simplicity. We consider spacetimes that are stationary, axisymmetric, and asymptotically flat. The

symmetries of stationarity and axisymmetry are associated with the existence of two Killing vector fields, one timelike at spatial infinity, t^α, and one spacelike everywhere and with closed orbits, φ^α.

It was shown by Carter [20] that under these assumptions the Killing vectors commute, and one can choose an adapted coordinate system (t, x^1, x^2, φ), such that $t^\alpha \partial_\alpha = \partial/\partial t$ and $\varphi^\alpha \partial_a = \partial/\partial\varphi$, i.e.

$$t^\alpha = (1,0,0,0)\,, \quad \text{and} \quad \varphi^\alpha = (0,0,0,1)\,. \tag{20}$$

We choose the remaining two coordinates to be of spherical type, i.e. $x^1 = r$, $x^2 = \theta$, and following Gourgoulhon et al. [21], we fix the gauge to be of maximal-slicing quasi-isotropic type (MSQI), for which the line element reads as

$$\begin{aligned} ds^2 &= g_{\alpha\beta}\, dx^\alpha dx^\beta = -(N^2 - N_\varphi N^\varphi)\, dt^2 - 2N_\varphi\, d\varphi\, dt \\ &\quad + A^2\left(dr^2 + r^2 d\theta^2\right) + B^2 r^2 \sin^2\theta\, d\varphi^2\,, \end{aligned} \tag{21}$$

where the functions N, N^φ, A and B depend on r and θ only, and $N_\varphi \equiv g_{\varphi\varphi} N^\varphi$.

B. Fluid dynamics

We assume the flow of the two fluids to be purely *axial* (i.e. no convective meridional currents), so we can write the unit 4–velocities of the two fluids as

$$u^\alpha_{\rm n} = u^t_{\rm n}\, \zeta^\alpha_{\rm n} \quad \text{and} \quad u^\alpha_{\rm p} = u^t_{\rm p}\, \zeta^\alpha_{\rm p}\,, \tag{22}$$

where the helical vectors $\zeta^\alpha_{\rm n}$ and $\zeta^\alpha_{\rm p}$ are expressible in terms of the Killing vectors t^α and φ^α as

$$\zeta^\alpha_{\rm n} = t^\alpha + \Omega_{\rm n}\varphi^\alpha\,, \quad \text{and} \quad \zeta^\alpha_{\rm p} = t^\alpha + \Omega_{\rm p}\varphi^\alpha\,, \tag{23}$$

where the two rotation rates $\Omega_{\rm n}$ and $\Omega_{\rm p}$ are scalar functions, which can only depend on r and θ.

Using Cartan's formula for the Lie derivative of a 1–form p_β with respect to a vector–field ξ^α, namely

$$\mathcal{L}_\xi\, p_\alpha = 2\xi^\beta \nabla_{[\beta} p_{\alpha]} + \nabla_\alpha\left(\xi^\beta p_\beta\right)\,, \tag{24}$$

we can rewrite the equations of motion (9) as

$$\mathcal{L}_{\zeta_X} \mathrm{p}^X_\alpha - \nabla_\alpha\left(\zeta^\beta_X \mathrm{p}^X_\beta\right) = 0\,. \tag{25}$$

Linearity of the Lie derivative together with (23) and (24) allows us to rewrite this as

$$\mathcal{L}_t\, p^X_\alpha + \Omega_X \mathcal{L}_\varphi\, p^X_\alpha + \varphi^\beta p^X_\beta\, \nabla_\alpha \Omega_X - \nabla_\alpha\left(\zeta^\beta_X p^X_\beta\right) = 0\,. \tag{26}$$

Stationarity and axisymmetry imply that the first two terms vanish, and so the equations of motion for neutrons and protons are reduced to

$$p^{\rm n}_\varphi \nabla_\alpha \Omega_{\rm n} = \nabla_\alpha\left(\zeta^\beta_{\rm n}\, p^{\rm n}_\beta\right)\,, \quad p^{\rm p}_\varphi \nabla_\alpha \Omega_{\rm p} = \nabla_\alpha\left(\zeta^\beta_{\rm p}\, p^{\rm p}_\beta\right)\,. \tag{27}$$

In the general case of differential rotation, the integrability condition of these equations are therefore

$$p^{\rm n}_\varphi = p^{\rm n}_\varphi(\Omega_{\rm n})\,, \quad \text{and} \quad p^{\rm p}_\varphi = p^{\rm p}_\varphi(\Omega_{\rm p})\,, \tag{28}$$

and the first integrals of motion are obtained as

$$p^{\rm n}_t + \Omega_{\rm n} p^{\rm n}_\varphi - \int^{\Omega_{\rm n}} p^{\rm n}_\varphi(\Omega')d\Omega' \;=\; \text{const}^{\rm n}\,, \tag{29}$$

$$p^{\rm p}_t + \Omega_{\rm p} p^{\rm p}_\varphi - \int^{\Omega_{\rm p}} p^{\rm p}_\varphi(\Omega')d\Omega' \;=\; \text{const}^{\rm p}\,. \tag{30}$$

In the special case of *uniform rotation*, i.e. $\nabla_\alpha \Omega_X = 0$, these first integrals reduce to

$$p^{\rm n}_t + \Omega_{\rm n} p^{\rm n}_\varphi = \text{const}^{\rm n}\,, \quad \text{and} \quad p^{\rm p}_t + \Omega_{\rm p} p^{\rm p}_\varphi = \text{const}^{\rm p}\,, \tag{31}$$

which are equivalent to the expressions obtained by Andersson and Comer [9]. We can further express these first integrals in terms of the chemical potentials $\mu^{\rm n}$, $\mu^{\rm p}$ of (17), namely

$$p^{\rm n}_t + \Omega_{\rm n} p^{\rm n}_\varphi \;=\; \zeta^\alpha_{\rm n} p^{\rm n}_\alpha = -\frac{1}{u^t_{\rm n}}\mu^{\rm n} = \text{const}^{\rm n}\,, \tag{32}$$

$$p^{\rm p}_t + \Omega_{\rm p} p^{\rm p}_\varphi \;=\; \zeta^\alpha_{\rm p} p^{\rm p}_\alpha = -\frac{1}{u^t_{\rm p}}\mu^{\rm p} = \text{const}^{\rm p}\,. \tag{33}$$

C. The $3+1$ decomposition

We introduce the vector $\mathfrak{n}^\alpha$ as the unit normal to the spacelike hypersurfaces Σ_t defined by $t = \text{const.}$, namely

$$\mathfrak{n}_\alpha \equiv -N \nabla_\alpha t\,, \tag{34}$$

which defines the so–called *Eulerian observers* $\mathcal{O}_0$ following Smarr and York [22]. The induced metric $h_{\alpha\beta}$ on the spacelike hypersurfaces Σ_t is given by the projection

$$h_{\alpha\beta} \equiv g_{\alpha\beta} + \mathfrak{n}_\alpha \mathfrak{n}_\beta\,. \tag{35}$$

The corresponding $3+1$ decomposition of the energy–momentum tensor $T^{\alpha\beta}$ reads as[4]

$$T^{\alpha\beta} = S^{\alpha\beta} + 2\mathfrak{n}^{(\alpha} J^{\beta)} + E\mathfrak{n}^\alpha \mathfrak{n}^\beta\,, \tag{36}$$

where

$$E = \mathfrak{n}^\alpha T_{\alpha\beta} \mathfrak{n}^\beta\,, \quad J_\alpha = -h^\gamma_\alpha T_{\gamma\beta}\mathfrak{n}^\beta\,, \quad S_{\alpha\beta} = h^\gamma_\alpha T_{\gamma\nu} h^\nu_\beta\,, \tag{37}$$

which can be interpreted as the energy, momentum and stress tensor as measured by the Eulerian observers. In the MSQI gauge (21), we can explicitly express these quantities as

$$E = N^2 T^{tt}\,, \quad J_i = N T^t_i\,, \quad S^i_j = T^i_j - N^i T^t_j\,, \tag{38}$$

---

[4] Round brackets denote averaged symmetrization, i.e. $2\,v_{(a,b)} = v_{ab} + v_{ba}$.

where Latin indices i, j denote the space-components $1, 2, 3$. The Einstein equations in this formulation result in a set of four elliptic equations for the metric potentials (see [23] and [21] for details), namely

$$\Delta_3 \nu = 4\pi A^2 (E + S_i^i) + A^2 K_{ij} K^{ij} - \partial\nu\, \partial(\nu + \beta), \quad (39)$$

$$\tilde{\Delta}_3 \widetilde{N}^\varphi = -16\pi N A^2 \widetilde{J}^\varphi - r \sin\theta\, \partial N^\varphi \partial(3\beta - \nu)\,, \quad (40)$$

$$\Delta_2[(NB-1) r \sin\theta] = 8\pi N A^2 B r \sin\theta \left(S_r^r + S_\theta^\theta\right), \quad (41)$$

$$\Delta_2 \left(\nu + \bar{\alpha}\right) = 8\pi A^2 S_\varphi^\varphi + \frac{3}{2} A^2 K_{ij} K^{ij} - (\partial\nu)^2 \,, \quad (42)$$

where we defined $\widetilde{N}^\varphi \equiv r \sin\theta\, N^\varphi$ and $\widetilde{J}^\varphi \equiv r \sin\theta\, J^\varphi$. Δ_3 and Δ_2 are the flat three- and two-dimensional Laplace operators, whereas $\tilde{\Delta}_3 = \Delta_3 - (r^2 \sin^2\theta)^{-1}$. We further used the notation

$$\nu \equiv \ln N\,, \quad \bar{\alpha} \equiv \ln A\,, \quad \beta \equiv \ln B\,, \quad (43)$$

and we define $\partial\bar{\alpha}\partial\beta$ as the flat-space scalar product of two gradients, i.e.

$$\partial\bar{\alpha}\partial\beta \equiv \partial_r \bar{\alpha} \partial_r \beta + \frac{1}{r^2} \partial_\theta \bar{\alpha} \partial_\theta \beta\,. \quad (44)$$

The only non-zero components of the extrinsic curvature K_{ij} in our spherical coordinate basis are given by

$$K_{r\varphi} = -\frac{g_{\varphi\varphi}}{2N}\, \partial_r N^\varphi\,, \quad \text{and} \quad K_{\theta\varphi} = -\frac{g_{\varphi\varphi}}{2N}\, \partial_\theta N^\varphi\,. \quad (45)$$

We note that the gravitational mass $\mathcal{M}$, which is defined as the (negative) coefficient of the term $1/r$ in an asymptotic expansion of the "gravitational potential" $\log N$, can be expressed explicitly (see [23]) as

$$\mathcal{M} = \int A^2 B \left[N(E + S_i^i) + 2B^2 \widetilde{N}^\varphi \widetilde{J}^\varphi\right] r^2 \sin\theta\, dr\, d\theta\, d\varphi\,. \quad (46)$$

Here and in the following we will use $\mathcal{M}$ to denote the gravitational mass, while M will stand for the baryon mass. The total angular momentum $\mathcal{J}$ is given by

$$\mathcal{J} = \int \left[A^2 B^3\, r \sin\theta \widetilde{J}^\varphi\right] r^2 \sin\theta\, dr\, d\theta\, d\varphi\,. \quad (47)$$

The 2D- and 3D virial identities, which have been derived by Bonazzola and Gourgoulhon [24, 25], can serve as a useful check of consistency and precision of the numerical results. The 2D virial identity (referred to as GRV2), which derives from the Poisson-equation (42), has the form

$$\int \left[8\pi A^2 S_\varphi^\varphi + \frac{3}{2} A^2 K_{ij} K^{ij} - (\partial\nu)^2\right] r\, dr\, d\theta = 0\,, \quad (48)$$

while the 3D virial identity (GRV3), which reduces to the usual virial theorem in the Newtonian limit, can be written as

$$\int 4\pi A^2 B S_i^i\, dV + \int B \left[\frac{3}{4} A^2 K_{ij} K^{ij} - (\partial\nu)^2 + \frac{1}{2}\, \partial\bar{\alpha}\partial\beta\right] dV + \int \frac{1}{2r} \left(B - \frac{A^2}{B}\right) \times \left[\partial_r \left(\bar{\alpha} - \beta/2\right) + \frac{1}{r \tan\theta} \partial_\theta \left(\bar{\alpha} - \beta/2\right)\right] = 0\,. \quad (49)$$

Both of these virial theorems (48) and (49) can be written as the sum of an integral over a "material" term $I_{\rm mat}$ (the first term in (48) and (49) respectively), and an integral over pure field-quantities $I_{\rm fields}$ (the remaining terms). Therefore it will be convenient to consider the following dimensionless quantity to numerically characterize the respective virial violations:

$$GRV \equiv \frac{I_{\rm mat} + I_{\rm fields}}{I_{\rm mat}}\,. \quad (50)$$

D. The matter sources

Let us write $\Gamma_{\rm n}$ and $\Gamma_{\rm p}$ for the two Lorentz factors linking the Eulerian observers $\mathcal{O}_0$ to the co-moving fluid observers $\mathcal{O}_{\rm n}$ (defined by $u_{\rm n}^\alpha$) and $\mathcal{O}_{\rm p}$ (defined by $u_{\rm p}^\alpha$), namely

$$\Gamma_{\rm n} \equiv -\mathfrak{n}_\alpha u_{\rm n}^\alpha = N u_{\rm n}^t\,, \quad \text{and} \quad \Gamma_{\rm p} \equiv -\mathfrak{n}_\alpha u_{\rm p}^\alpha = N u_{\rm p}^t\,. \quad (51)$$

The "physical" fluid velocities $U_{\rm n}$ and $U_{\rm p}$ of the two fluids[5] in the φ direction, as measured by $\mathcal{O}_0$, are given by

$$U_{\rm n} = \frac{1}{\Gamma_{\rm n}} \hat{\varphi}_\alpha u_{\rm n}^\alpha\,, \quad \text{and} \quad U_{\rm p} = \frac{1}{\Gamma_{\rm p}} \hat{\varphi}_\alpha u_{\rm p}^\alpha\,, \quad (52)$$

where $\hat{\varphi}^\alpha$ is the *spatial* unit vector in the φ direction, i.e.

$$\hat{\varphi}^\alpha = \frac{1}{\sqrt{g_{\varphi\varphi}}}\, \varphi^\alpha\,, \quad \text{such that} \quad h_{\alpha\beta}\, \hat{\varphi}^\alpha \hat{\varphi}^\beta = 1\,. \quad (53)$$

Using (22) and (51), we obtain

$$U_{\rm n} = \frac{\sqrt{g_{\varphi\varphi}}}{N} \left(\Omega_{\rm n} - N^\varphi\right),\; U_{\rm p} = \frac{\sqrt{g_{\varphi\varphi}}}{N} \left(\Omega_{\rm p} - N^\varphi\right)\,, \quad (54)$$

and the Lorentz factors can be expressed equivalently as

$$\Gamma_{\rm n} = \left(1 - U_{\rm n}^2\right)^{-1/2}\,, \quad \text{and} \quad \Gamma_{\rm p} = \left(1 - U_{\rm p}^2\right)^{-1/2}\,. \quad (55)$$

The "crossed" scalar x^2, defined in (2), can be expressed in terms of the respective scalar particle densities $n_{\rm n}$, $n_{\rm p}$ and the 3–velocities $U_{\rm n}$ and $U_{\rm p}$, as

$$x^2 = n_{\rm n} n_{\rm p} \frac{1 - U_{\rm n} U_{\rm p}}{\sqrt{(1 - U_{\rm n}^2)(1 - U_{\rm p}^2)}}\,, \quad (56)$$

[5] In Andersson and Comer [9] these were denoted $-\omega_{\rm n}$ and $-\omega_{\rm p}$ respectively.

and using (14), we can write the relative velocity Δ as

$$\Delta^2 = \frac{(U_{\rm n} - U_{\rm p})^2}{(1 - U_{\rm n}U_{\rm p})^2}\,. \tag{57}$$

Using expressions (32),(33) and (51), the first integrals can be cast into the form

$$\frac{N}{\Gamma_{\rm n}}\mu^{\rm n} = {\rm const}^{\rm n}\,, \quad \text{and} \quad \frac{N}{\Gamma_{\rm p}}\mu^{\rm p} = {\rm const}^{\rm p}\,. \tag{58}$$

In closer analogy with [21, 23], we can alternatively write these first integrals as

$$H_{\rm n} + \nu - \ln\Gamma_{\rm n} = \mathcal{C}_{\rm n}\,, \tag{59}$$
$$H_{\rm p} + \nu - \ln\Gamma_{\rm p} = \mathcal{C}_{\rm p}\,, \tag{60}$$

where we introduced the abbreviations

$$H_{\rm n} \equiv \ln\left(\frac{\mu_{\rm n}}{m^{\rm n}}\right)\,, \quad \text{and} \quad H_{\rm p} \equiv \ln\left(\frac{\mu_{\rm p}}{m^{\rm p}}\right)\,. \tag{61}$$

The components of the $3+1$ decomposition (36) of the energy–momentum tensor (10) are explicitly found as

$$E = -\Psi + (\Gamma_{\rm n}^2\mathcal{K}^{\rm nn}n_{\rm n}^2 + \Gamma_{\rm p}^2\mathcal{K}^{\rm pp}n_{\rm p}^2 + 2\Gamma_{\rm n}\Gamma_{\rm p}\mathcal{K}^{\rm np}n_{\rm n}n_{\rm p})\,, \tag{62}$$
$$\sqrt{g_{\varphi\varphi}}\,J^{\varphi} = \Gamma_{\rm n}^2\mathcal{K}^{\rm nn}n_{\rm n}^2U_{\rm n} + \Gamma_{\rm p}^2\mathcal{K}^{\rm pp}n_{\rm p}^2U_{\rm p} + \Gamma_{\rm n}\Gamma_{\rm p}\mathcal{K}^{\rm np}n_{\rm n}n_{\rm p}(U_{\rm n} + U_{\rm p})\,, \tag{63}$$
$$S^r_r = S^\theta_\theta = \Psi\,, \tag{64}$$
$$S^\varphi_\varphi = \Psi + \big(\Gamma_{\rm n}^2\mathcal{K}^{\rm nn}n_{\rm n}^2U_{\rm n}^2 + \Gamma_{\rm p}^2\mathcal{K}^{\rm pp}n_{\rm p}^2U_{\rm p}^2 + 2\Gamma_{\rm n}\Gamma_{\rm p}\mathcal{K}^{\rm np}n_{\rm n}n_{\rm p}U_{\rm n}U_{\rm p}\big)\,, \tag{65}$$

One can check the consistency of this result with the single fluid case of [23], by considering the special case of both fluids moving together.

IV. NUMERICAL PROCEDURE

A. Iteration scheme

The numerical solution of the stationary axisymmetric configurations described in the previous sections proceeds in a very similar manner to the single-fluid case, which is described in more detail in [21, 23]. The central iteration scheme is nearly identical:

Initialization: Start from a simple "guess" for a spherically symmetric matter distribution $n_{\rm n}^{(0)}$ and $n_{\rm p}^{(0)}$ of the two fluids, and use a flat metric.

Step 1: Calculate the matter source-terms E, J^φ and $\mathcal{S}^i_j$ from (62)– (65).

Step 2: Solve the equations (39)–(42) for the corresponding metric using the pseudo-spectral elliptic solver in LORENE, the numerical relativity package used here[26].

Step 3: Use the first integrals (58) to obtain the chemical potentials $\mu^{\rm n}$ and $\mu^{\rm p}$.

Step 4: Calculate the new density fields $n_{\rm n}$ and $n_{\rm p}$ by inverting the relations (17) for the given equation of state.

Step 5: Continue at Step 1 until the desired convergence is achieved.

In general we are using three spherical-type numerical domains to cover the hypersurface Σ_t: the innermost domain covers the whole star. An intermediate domain is used for the vicinity of the star to about twice the stellar radius, and an outer domain covers the space out to infinity, using a compactification of the type $u = 1/r$ (see [23] for details). For the inner domain we have the choice of either using a simple spherical grid containing the whole star, or we can use an adaptive-grid algorithm, in order to adapt the domain-boundary to the stellar surface. Contrary to the single-fluid case (e.g. see [21]), however, the adaptive-grid approach is much less effective in increasing precision and convergence. The reason for this is simply that only one of the two fluid-surfaces can be matched up with a domain boundary, and therefore the (weak) Gibbs phenomenon due to the inner fluid surface (representing at least a discontinuity in the derivative) is not completely avoidable.

Another important difference in the case of two-fluids compared to single-fluid stars is the way we determine the location of the fluid surfaces. In a single fluid star, the surface can always be found by the vanishing of the pressure, which usually translates into a simple condition in terms of the vanishing of the chemical potential μ. In the two-fluid case, however, this is not generally possible (especially for the "inner" fluid), due to the coupling of the fluids. Therefore we need to define the fluid surfaces directly in terms of the vanishing of the respective density fields. Contrary to the chemical potential, the density can have a vanishing or diverging gradient at the surface, and a precise determination of the surface can therefore be numerically difficult.[6]

A related numerical problem specific to two-fluid configurations appears when the surfaces of the two fluids are very close to each other. In this case, the 1-fluid region in between the two surfaces will be poorly resolved by the grid covering the star, and therefore the determination of the outer surface will have a poor numerical precision. As will be seen later, this problem can be cured to some extent by adding another domain, which covers just a thin shell below and up to the outer fluid surface. In this case one observes a drastic improvement in the precision

[6] We note that Yoshida and Eriguchi [11] chose to avoid this difficulty by *defining* the "fluid surfaces" by the vanishing of the respective chemical potentials. These "surfaces", however, do generally *not* coincide with the surfaces of vanishing density (contrary to the single-fluid case), as can be seen from (17).

of finding the outer surface, which can be quantified by comparison with the analytic slow-rotation solution.

We note that this numerical code can be used equally well for Newtonian configurations, simply by replacing the matter-sources by their Newtonian limits, and forcing the spatial metric to be flat. The central iteration scheme remains unchanged, and we can relate the lapse N to the Newtonian gravitational potential, namely by the relation $\nu = \ln N = \Phi/c^2$, where Φ is the Newtonian gravitational potential. The Newtonian limit of the matter source-term in Eq. (39) is

$$\frac{E + S_i^i}{c^2} = \rho + \mathcal{O}(c^{-2})\,, \tag{66}$$

where ρ is the total (rest-)mass-density, so that this component of the Einstein equations reduces to the Newtonian Poisson equation, while the remaining Einstein equations (40)–(42) become trivial in this limit. In a similar manner, the first integrals are seen to reduce exactly to their Newtonian counterparts [10].

The parameters of the numerical scheme that will be used for the rest of the paper are the following: the required convergence of the iteration scheme is 10^{-10}, and we use 17 points in the θ direction, and 33 grid-points in the radial direction in the innermost domain (containing the star), 33 radial points in the intermediate domain and 17 radial points in the compactified outer domain.

B. The polytropic 2-fluid equation of state

The numerical scheme described in the previous section can be used for any invertible 2-fluid equation of state (EOS). The current implementation of our code, however, only covers a "polytropic" subclass of 2-fluid EOS, which generalizes the types of EOS used in previous studies, e.g. [9–11, 27], and which has the general form

$$\begin{aligned}\mathcal{E} \;=\; & \rho\, c^2 + \frac{1}{2}\kappa_{\rm n} {\rm n}^{\gamma_1} + \frac{1}{2}\kappa_{\rm p} n_{\rm p}^{\gamma_2} + \kappa_{\rm np} n_{\rm n}^{\gamma_3} n_{\rm p}^{\gamma_4} \\ & + \kappa_{\scriptscriptstyle\Delta}\, n_{\rm n}^{\gamma_5} n_{\rm p}^{\gamma_6} \Delta^2\,,\end{aligned} \tag{67}$$

where $\rho \equiv m_{\rm n} n_{\rm n} + m_{\rm p} n_{\rm p}$. As discussed in the introduction, we expect this polytropic EOS-class to be quite general, and to allow one to study the qualitative features of a broad range of different superfluid neutron star models. For example, general features of the Kepler limit (cf. Fig. 5) are seen to be in qualitative agreement with the mean field results of Comer [12].

The two fluids in (67) are coupled via a "symmetry energy"-type term proportional to $\kappa_{\rm np}$ and an entrainment term proportional to $\kappa_{\scriptscriptstyle\Delta}\Delta^2$. The resulting expressions for the chemical potentials and the entrainment α are directly obtainable from (15).

In general this class of 2-fluid EOS requires a numerical inversion in the iteration scheme described in section IV A, in order to obtain the densities $n_{\rm n}, n_{\rm p}$ from the chemical potentials $\mu^{\rm n}, \mu^{\rm p}$ at a given relative speed Δ. For testing purposes and for comparison to the Newtonian and relativistic slow-rotation results, we will in the following be mostly interested in a further subclass of the above EOS, namely the special 2-fluid polytropes described by

$$\mathcal{E} = \rho\, c^2 + \frac{1}{2}\kappa_{\rm n} n_{\rm n}^2 + \frac{1}{2}\kappa_{\rm p} n_{\rm p}^2 + \kappa_{\rm np} n_{\rm n} n_{\rm p} + \kappa_{\scriptscriptstyle\Delta}\, n_{\rm n} n_{\rm p} \Delta^2\,, \tag{68}$$

which are a 2-fluid generalization of the 1-fluid polytrope $P \propto n^2$. This special EOS class still exhibits all the coupling-types (entrainment + symmetry energy) of the general EOS, but allows an analytic inversion, namely

$$\mu^{\rm n} - m_{\rm n} c^2 \;=\; \kappa_{\rm n} n_{\rm n} + (\kappa_{\rm np} + \kappa_{\scriptscriptstyle\Delta}\Delta^2)\, n_{\rm p}\,, \tag{69}$$

$$\mu^{\rm p} - m_{\rm p} c^2 \;=\; \kappa_{\rm p} n_{\rm p} + (\kappa_{\rm np} + \kappa_{\scriptscriptstyle\Delta}\Delta^2)\, n_{\rm n}\,, \tag{70}$$

and the entrainment is found as

$$\alpha = \kappa_{\scriptscriptstyle\Delta}\, n_{\rm n} n_{\rm p}\,. \tag{71}$$

The generalized pressure Ψ in (19) is expressible as

$$\Psi = \frac{1}{2}\kappa_{\rm n} {\rm n}^2 + \frac{1}{2}\kappa_{\rm p} n_{\rm p}^2 + \kappa_{\rm np} n_{\rm n} n_{\rm p} + \kappa_{\scriptscriptstyle\Delta}\, n_{\rm n} n_{\rm p} \Delta^2\,. \tag{72}$$

Contrary to the two-fluid EOS used in the Newtonian slow-rotation study [10], which exhibits the somewhat unphysical feature of constant entrainment numbers, as discussed in appendix A, this EOS results in a much more physical behavior of the entrainment. Namely, using (16), we find

$$\varepsilon_{\rm n} = \frac{2\kappa_{\scriptscriptstyle\Delta}}{m^{\rm n}}\, n_{\rm p}\,, \quad \text{and} \quad \varepsilon_{\rm p} = \frac{2\kappa_{\scriptscriptstyle\Delta}}{m^{\rm p}}\, n_{\rm n}\,, \tag{73}$$

which ensures that the entrainment effect automatically vanishes when one of the two fluid-densities goes to zero. Such a linear behavior of entrainment also happens to be in quite good qualitative agreement with the theoretical predictions of nuclear physics, e.g. see[7] [2, 3, 28]

Using the method developed in [10] for the EOS (68), we can find an analytic solution in the Newtonian slow-rotation approach, which is presented in appendix A. This allows us to run extensive tests by comparing our numerical code to the analytic solution in the Newtonian case. The results of this comparison are presented in section V C.

V. TESTS OF THE NUMERICAL CODE

A. Comparison to 1-fluid results

As a first consistency check we use the two-fluid code for strictly co-rotating configurations with a common

[7] These references give the neutron and proton effective masses m^{X*}, which are related to the entrainment via $\varepsilon_X = (m^X - m^{X*})/m^X$, see [10] for details.

outer surface, and compare the results to those of the well-tested single-fluid code [21, 23]. For this purpose we study a stellar sequence of fixed central density and vary the rotation rate. We define the "natural scale" of the rotation-rate as

$$\Omega_0 \equiv \sqrt{4\pi G\,\rho(0)}\,, \tag{74}$$

where $\rho(0)$ is the central rest-mass density, i.e. $\rho(0) = m^{\rm n} n_{\rm n}(0) + m^{\rm p} n_{\rm p}(0)$. The Kepler rotation rate $\Omega_{\rm K}$ is typically found at about $\Omega_{\rm K} \sim 0.1\,\Omega_0$ for the configurations considered here. The results of the comparison with the single-fluid case are shown in Fig. 1. Here we plot the relative differences, defined as

$$\Delta Q \equiv \frac{|Q^{\rm 2f} - Q^{\rm 1f}|}{Q^{\rm 1f}}\,, \tag{75}$$

of a global quantity Q in the two-fluid case ($Q^{\rm 2f}$) and in the single-fluid case ($Q^{\rm 1f}$). The first column, figures 1 (a) and (c), shows the comparison of 1-fluid and 2-fluid results using a *fixed* spherical grid for the inner domain in the two-fluid case. The single-fluid code on the other hand always uses an adaptive grid for the stellar surface. We notice that towards higher rotation rates the relative errors increase. These errors can be entirely ascribed to the lack of grid adaption in the two-fluid case: by using an adaptive grid for the stellar domain also in the two-fluid case, we find a consistent agreement of better than 10^{-9}, as can be seen in the second column in figure 1 (b) and (d). We note, however, that this improvement of using an adaptive grid is restricted to cases where the two-fluids share a common outer surface, while it is of much less use in the general two-fluid case as mentioned earlier. We can therefore conclude that the two-fluid code reproduces results consistent with the single-fluid code in cases where the two fluids co-rotate.

B. Virial theorem violation

In the next step we consider the more general case where the two fluids have different rotation rates. We fix the relative rotation rate, defined as

$$\mathcal{R} \equiv \frac{\Omega_{\rm n} - \Omega_{\rm p}}{\Omega_{\rm p}}\,, \tag{76}$$

to be $\mathcal{R} = 1.51$ and vary $\Omega_{\rm n}$. As mentioned before, in these general situations an adaptive grid does not substantially improve the precision and has therefore not been used. We consider the internal consistency check provided by the virial identities GRV2 and GRV3 defined in (50), for which the result is shown in Fig. 2. We note that in the case (a), where one inner domain is used to cover the star, even at low rotation rates the result falls somewhat short of the convergence-goal of 10^{-10} in the iteration scheme. This lack of precision at small rotation rates can be understood as follows: due to the difference in rotation rates, the two fluids do not share a common outer surface, and there will necessarily be a 1-fluid region close to the outer surface. However, this 1-fluid region will be very thin compared to the dimensions of the star, and will therefore be poorly resolved in terms of the numerical grid. We can improve this by choosing a second domain to cover just a thin layer (of about 1% of the radius) below the outer surface, resolved by another 33 radial grid-points. The effect of this "trick" is rather impressive and can be seen in Fig. 2, for the case (b). While this gain in precision is not very important by itself, it underlines the consistency of the results and shows that the source of these errors is understood. The decrease in precision when approaching the Kepler rotation can be ascribed to the appearance of cusps at the equator (see Fig. 6) and therefore the presence of the Gibbs phenomenon. Nevertheless, one should note that this phenomenon happens also in the one-fluid case, the precision of the code at the Kepler limit being of the same order as here [21].

C. Comparison to Newtonian slow-rotation results

We can use the analytic Newtonian solution in the slow-rotation approximation (derived in appendix A) for a systematic comparison with the numerical code run in "Newtonian mode" as described in section IV A.

We denote the numerical solution of a quantity as $Q_{\rm L}(\Omega_X)$, and the analytic slow-rotation solution as $Q_{\rm sr}(\Omega_X)$, and we define the relative difference as

$$\diamond Q \equiv \frac{Q_{\rm L} - Q_{\rm sr}}{Q^{(0)}}\,, \tag{77}$$

where $Q^{(0)}$ corresponds to the static solution. At fixed relative rotation rate $\mathcal{R}$, the slow-rotation solution can be written as

$$Q_{\rm sr}(\Omega_{\rm n}) = Q^{(0)} + Q^{(2)}\,\Omega_{\rm n}^2\,. \tag{78}$$

Ideally we would like to compare only up to the Ω^2 component of the numerical solution, but obviously we do not know its Taylor-expansion in orders of Ω. Nevertheless the numerical solution can formally be written as

$$Q_{\rm L}(\Omega_{\rm n}) = Q_{\rm L}^{(0)} + Q_{\rm L}^{(2)}\,\Omega_{\rm n}^2 + Q_{\rm L}^{(4)}\,\Omega_{\rm n}^4 + \ldots\,, \tag{79}$$

so that the relative difference (77) can be expanded as

$$\diamond Q = \frac{Q_{\rm L}^{(0)} - Q^{(0)}}{Q^{(0)}} + \frac{Q_{\rm L}^{(2)} - Q^{(2)}}{Q^{(0)}}\,\Omega_{\rm n}^2 + \frac{Q_{\rm L}^{(4)}}{Q^{(0)}}\,\Omega_{\rm n}^4 + \ldots\,. \tag{80}$$

If the numerical solution agreed perfectly with the analytic solution (up to order Ω^2), the first two terms would be zero, and the leading order of the difference would be $\Omega_{\rm n}^4$. In practice, however, there will be contributions on all orders, and we will try to quantify these respective

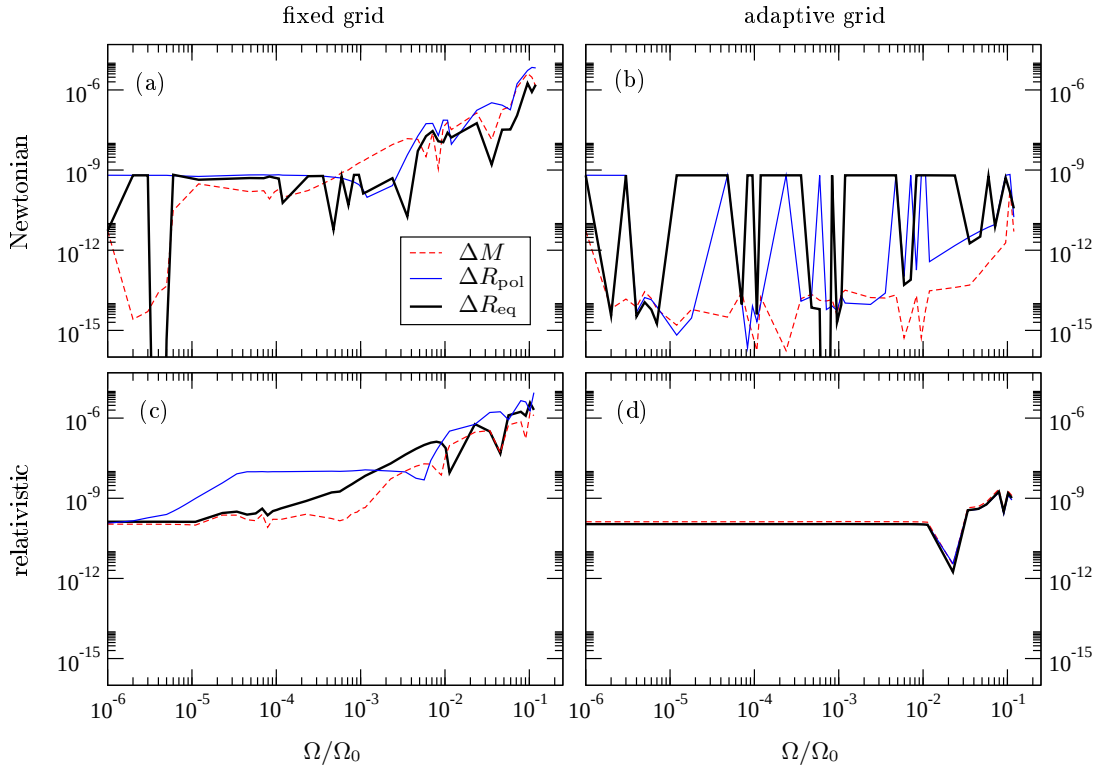

FIG. 1: Relative differences ΔQ in the total baryon mass M, and the equatorial and polar radii $R_{\rm eq}$ and $R_{\rm pol}$. The first row is the Newtonian case, while the second row shows the relativistic results. In the first column, we used a fixed spherical inner domain, while in the second column the inner domain-grid is adapted to the stellar surface (which is the default in the single-fluid case).

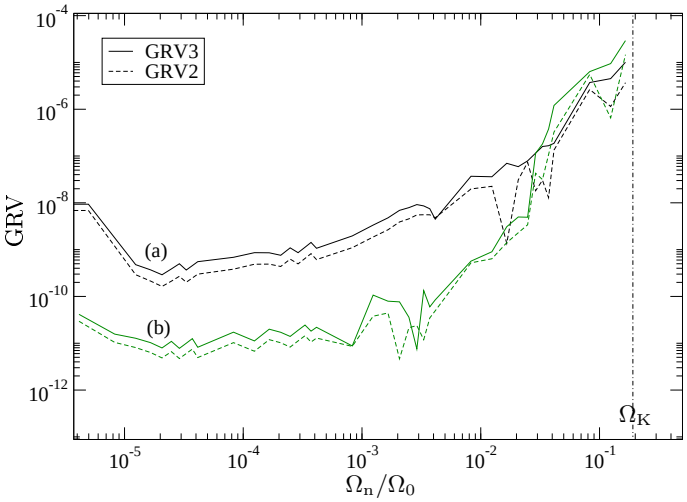

FIG. 2: Virial violations GRV2 and GRV3 for (a) 1 domain and (b) 2 domains covering the star. Only the Newtonian case is shown, as the relativistic results are very similar. $\Omega_{\rm K}$ denotes the Kepler rotation rate.

errors. If in some interval of $\Omega_{\rm n}$ one of these terms dominates in the series, then a log-log plot of $\diamond Q(\Omega_{\rm n})$ in this region would look like

$$y = \log(a\,\Omega_{\rm n}^m) = \log a + m\,\log\Omega_{\rm n}\,, \qquad (81)$$

i.e. a straight line with steepness m and an offset $\log a$. Conversely, if the log-log plot of $\diamond Q$ contains sections of straight lines, we can infer the leading power in $\Omega_{\rm n}$ and its coefficient.

The neutron-star model used here is characterized by the following choice of EOS-parameters:

$$\kappa_{\rm n} = 0.02\,,\ \kappa_{\rm p} = 0.12\,,\ \kappa_{\rm np} = 0.01\,,\ \kappa_\Delta = 0.02\,, \qquad (82)$$

and the (fixed) central chemical potentials

$$\mu^{\rm n}(0) = \mu^{\rm p}(0) = 0.2\,m_b\,c^2\,, \qquad (83)$$

where $m_b = 1.66\times10^{-27}$ kg is the baryon mass and c is the speed of light. The resulting neutron-star model in the static case has a total mass of $M = 1.50\,M_\odot$ (where $M_\odot$ is the solar mass), a radius of $R = 11.1$ km, a central baryon number density $\mathrm{n}(0) = 1.04$ fm^{-3}, proton fraction $x_{\rm p} \equiv n_{\rm p}/n = 0.083$ and an entrainment value of $\varepsilon_{\rm p}(0) = 0.38$. We note that in the Newtonian case there is no distinction between the gravitational mass $\mathcal{M}$ and the baryon mass M.

In Fig. 3 we show the relative differences $\diamond Q$ for the radii $R_{\rm n}$ and $R_{\rm p}$ at the equator. We also plotted the

straight lines corresponding to a pure Ω^4 and Ω^2 behavior, in order to facilitate the interpretation of these results.

In Fig. 3 (a) we see that for small rotation rates ($\Omega_{\rm n}/\Omega_0 < 10^{-3}$) the error in the equatorial proton radius $R_{\rm p}({\rm eq})$ reaches a "plateau" at about $\sim 10^{-9}$, which corresponds to numerical errors and the finite convergence-condition of the iteration scheme, while for higher rotation rates, the quartic error starts to dominate. The same behavior is observed for other global quantities, e.g. $M_{\rm n}$ and $M_{\rm p}$ and $R({\rm pol})$), which are not included in this plot. However, the neutron equatorial radius $R_{\rm n}({\rm eq})$ (which is the outer radius) displays a consistent *quadratic* error of order unity! The reason for this apparent discrepancy is rather subtle, and stems from the somewhat different nature of the slow-rotation approach and the fully numerical solution. In the numerical code, when one of the two fluid-densities vanishes, we switch from the 2-fluid EOS (67) to the corresponding 1-fluid EOS *before* we do the inversion $\mu^X \to n_Y$ in the numerical procedure (cf. section IV A), which is the correct physical way to do this. In the slow-rotation approach, however, the rotation rates are treated as infinitesimal, and there is actually no finite 1-fluid region. Therefore the EOS is always used in the form (67), which will be seen in the following to account for the difference in $R_{\rm n}({\rm eq})$. In order to test this explanation, we have also implemented a "slow-rotation style" EOS-inversion in the code, in which we *do not* switch to a 1-fluid EOS when one of the two fluids vanishes. The result of this is shown in Fig. 3 (b). We see that the discrepancy of the outer radius has completely disappeared. While this serves as an interesting test of consistency, this rather unphysical EOS-inversion will obviously not be used in the following.

D. Comparison to relativistic slow-rotation results

Finally, we compare our results in the fully relativistic case to the results obtained by using a code developed by Andersson and Comer [9], which is based on the relativistic slow-rotation approximation.

In the relativistic case the physical "radius" will generally be different from the coordinate-radius, and can be defined in various non-equivalent ways (e.g. circumferential radius, proper radius). For an unambiguous comparison we define the "radius" R as the proper distance of the surface from the center of the star, along a line of constant θ and φ (the definition of which is consistent with [9]), i.e.

$$R \equiv \int_0^{R_0} d\,l = \int_0^{R_0} A(r)\, d\,r\,, \tag{84}$$

where R_0 is the coordinate-radius of the surface. Another quantity specific to the relativistic case is the shift-vector $N^i = (0, 0, N^\varphi)$, and we will consider its 3-norm, i.e.

$$||N^i|| \equiv \sqrt{g_{ij} N^i N^j} = N^\varphi \sqrt{g_{\varphi\varphi}}\,, \tag{85}$$

which is independent of the coordinate-system chosen on the spacelike hypersurface.

The stellar model used in this comparison is defined by the EOS parameters

$$\kappa_{\rm n} = 0.04\,,\ \kappa_{\rm p} = 0.24\,,\ \kappa_{\rm np} = 0.02\,,\ \kappa_\Delta = 0.02\,, \tag{86}$$

and the central chemical potentials are $\mu^{\rm n}(0) = \mu^{\rm p}(0) = 0.2\, m_b\, c^2$. The configurations obtained have the following (fixed) central values: the central baryon density is ${\rm n}(0) = 0.5776\ {\rm fm}^{-3}$, which corresponds to 3.61 times nuclear density ($n_{\rm nucl} = 0.16\ {\rm fm}^{-3}$). The central proton entrainment is $\varepsilon_{\rm p}(0) = 0.212$, and the proton fraction is found as $x_{\rm p}(0) = 0.083$. We fix the relative rotation to $\mathcal{R} = 0.5$, i.e. the neutron superfluid is rotating 50% faster than the proton-electron fluid. In Table I we show the results of the comparison to the relativistic slow-rotation code. We observe that generally the agreement is quite good, and (as expected) gets worse with higher rotation rates. However, we note that this slow-rotation code imposes an additional constraint on the radii, namely the two fluids are forced to share a common outer surface. Therefore part of the disagreement observed here does not actually stem from the slow-rotation approximation or numerical differences, but from the somewhat different assumptions in the model. Given these differences, the agreement seems very good.

$\Omega_{\rm n}/2\pi$	0 Hz	100 Hz	500 Hz
$M_{\rm n}\,[M_\odot]$	1.0978 (-0.02%)	1.0998 (-0.1%)	1.1509 (-2%)
$M_{\rm p}\,[M_\odot]$	0.0998 (-0.02%)	0.0997 (-0.1%)	0.0959 (-2%)
$\mathcal{M}\,[M_\odot]$	1.1194 (-0.02%)	1.1210 (-0.04%)	1.1644 (0.04%)
$R_{\rm n}^{\rm eq}$ [km]	13.545 (-0.01%)	13.570 (0.2%)	14.260 (5%)
$R_{\rm n}^{\rm pol}$ [km]	13.545 (-0.01%)	13.527 (-0.1%)	13.103 (-3%)
$R_{\rm p}^{\rm eq}$ [km]	13.545 (-0.01%)	13.534 (-0.1%)	13.302 (-2%)
$R_{\rm p}^{\rm pol}$ [km]	13.545 (-0.01%)	13.527 (-0.1%)	13.103 (-3%)
$N(0)$	0.700102 (1e-4%)	0.69983 (2e-3%)	0.69267(-0.04%)
$\|\|N^i\|\|$(eq)	0	0.00206 (0.1%)	0.01072 (3%)

TABLE I: Numerical results $Q_{\rm L}$ and (in parentheses) relative differences $(Q_{\rm L} - Q_{\rm sr})/Q_{\rm L} \times 100\%$ to the relativistic slow-rotation results $Q_{\rm sr}$.

VI. NUMERICAL RESULTS

The existence of configurations with one fluid-surface having a prolate shape was initially found using the Newtonian analytic solution[10] in the slow-rotation approximation. While this might not be very realistic astrophysically, it is still interesting to study this particularity of an interacting two-fluid system. We confirm the existence of such configurations in the fully relativistic treatment, as reported earlier by us[14]. In order to show this, we choose the polytropic EOS parameters $\kappa_{\rm n} = 0.016$, $\kappa_{\rm p} = 0.16$, $\kappa_{\rm np} = 0.008$, and $\kappa_\Delta = 0.03$,

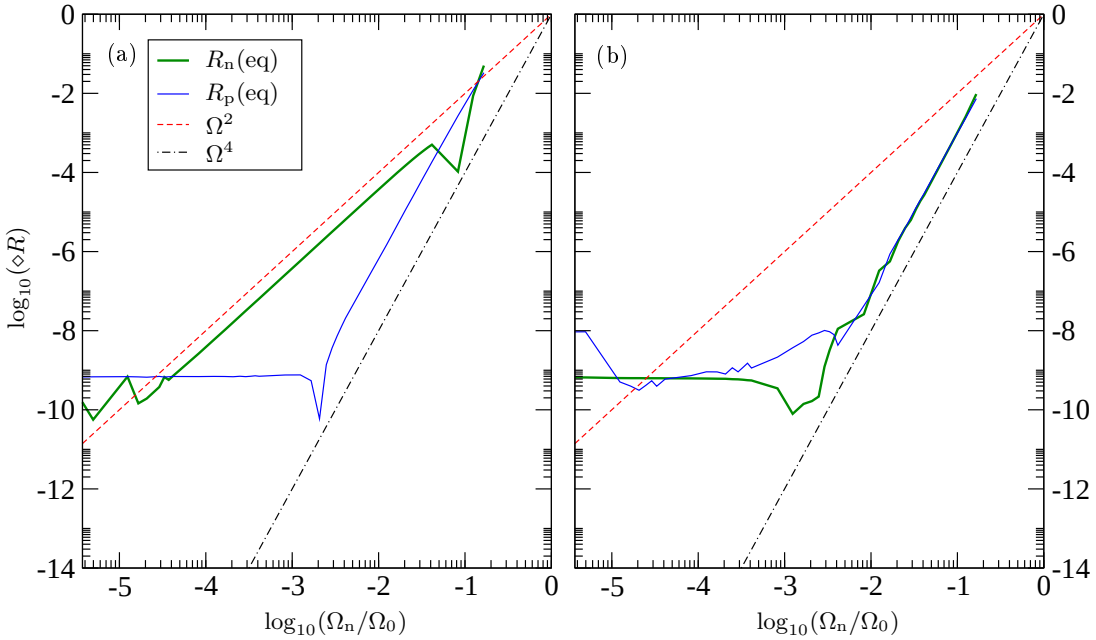

FIG. 3: Relative difference $\diamond Q(\Omega_n)$ between the numerical code in "Newtonian mode" and the slow-rotation analytic solution of appendix A, for the equatorial radii R_n and R_p. In (a) we used the normal "physical" EOS-inversion, while (b) shows the results when using a "slow-rotation style" EOS inversion.

with the central chemical potentials $\mu^n(0) = 0.2 m_b c^2$ and $\mu_p(0) = 0.198 m_b c^2$. This corresponds to a central proton fraction of $x_p(0) = 0.05$ and a central proton-entrainment number of $\varepsilon_p(0) = 0.80$. In Fig. 4 we show the resulting configuration with the two fluids counter-rotating at $\Omega_n/2\pi = 1000$ Hz and $\Omega_p/2\pi = -100$ Hz. We define the

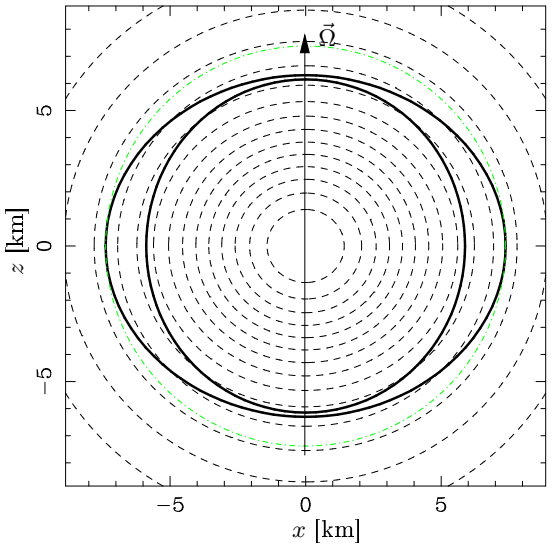

FIG. 4: Meridional cross-section of an oblate-prolate two-fluid configuration. The dotted lines represent lines of constant "gravitational potential" N, while the thick lines are the respective surfaces of the neutron- and proton fluids.

ellipticity of fluid X as

$$\epsilon_X \equiv \frac{R_X(\text{eq}) - R_X(\text{pol})}{R_X(\text{eq})}\,, \tag{87}$$

in terms of the proper radii R of (84). Using this definition, this configuration is found to have $\epsilon_n = 0.137$, and $\epsilon_p = -0.037$, so the proton fluid has a prolate shape despite the fact that it is rotating around the z-axis. This is made possible by the effective interaction potential created by the neutron-fluid, which "squeezes" the proton-fluid, in this case to the point of even overcoming the centrifugal potential.

EOS	κ_n	κ_p	κ_{np}	κ_Δ
I	0.05	0.5	0.025	0.02
II	0.05	0.5	0.0	0.0
III	0.05	0.5	−0.025	0.02

TABLE II: Polytropic parameters defining EOS-models I, II, and III

To simplify the presentation of results, we focus in the following on three EOS-models, defined in table II, which differ only by their interaction-terms. The EOS-models I and III differ by the sign of the "symmetry-interaction" term κ_{np}, which corresponds to a value of the canonical "symmetry-energy term" (introduced in Prix et al. [10]) of $\sigma = -0.5$ for EOS I and $\sigma = 0.5$ for EOS III. EOS II represents two fluids without EOS-interactions. If not otherwise stated, we choose the central chemical potentials as $\mu_n = \mu_p = 0.3\, m_b\, c^2$. In the static case we

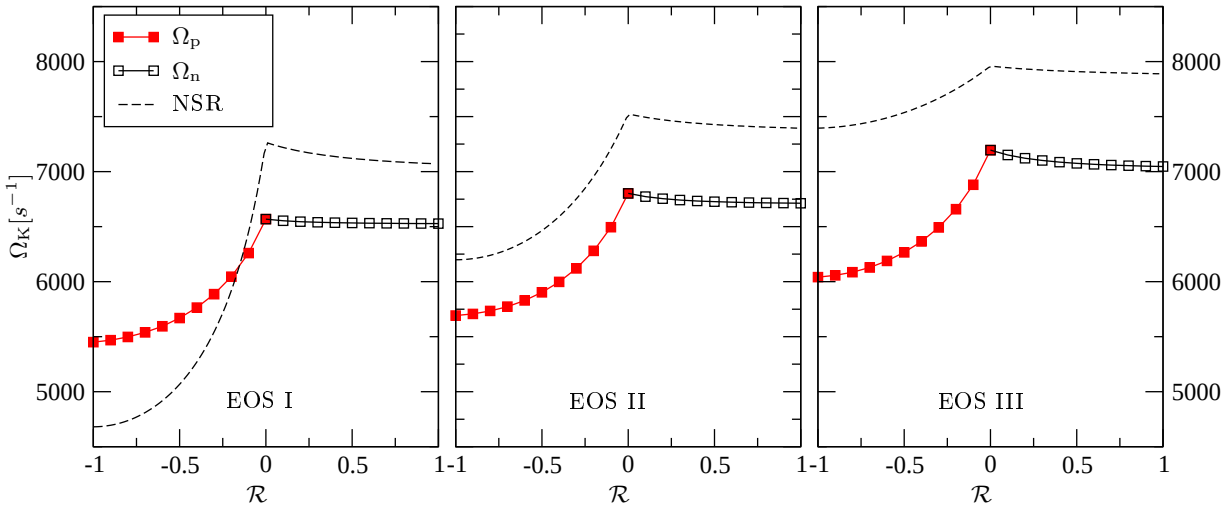

FIG. 5: Kepler limit Ω_K as a function of relative rotation rate $\mathcal{R}$ for EOS-models I, II and III. The dashed line (NSR) represents the result from the analytic Newtonian slow-rotation solution (cf. Appendix A)

obtain the results shown in Table III for these three EOS-models. We note that all three static configurations are on the stable branch of the mass-density relation, which can be seen in Fig. 7 for EOS-model I. We note that

	EOS I	EOS II	EOS III
n_c [fm^{-3}]	0.7177	0.7697	0.8612
$\varepsilon_p(0)$	0.273	0.0	0.301
$x_p(0)$	0.05	0.09	0.125
M [$M_\odot$]	1.586	1.532	1.448
$\mathcal{M}$ [$M_\odot$]	1.460	1.409	1.332
R [km]	14.37	13.88	13.12

TABLE III: Results for the central baryon number density n_c, entrainment ε_p, proton fraction x_p, total baryon mass M, gravitational mass $\mathcal{M}$ and the proper radius R for EOS-models I, II and III in the static case.

when considering rotation, the individual fluid radii will obviously change, but also the masses, because we only consider stellar sequences of fixed central density.

Next we consider these stellar models rotating at their maximum rotation rate Ω_K (called Kepler limit) for different relative rotation rates $\mathcal{R}$, as shown in Fig. 5. We define the Kepler-rate Ω_K as the rotation rate of the outer fluid (which in this case also happens to be the faster rotating one), i.e. the protons for $\mathcal{R} < 0$ and the neutrons for $\mathcal{R} > 0$. The rotation rate of the (slower) inner fluid is trivially determined by Ω_K and $\mathcal{R}$. The dashed line shows the result from the Newtonian slow-rotation solution (A42). This is seen to overestimates the Kepler rate typically by about 15 %, except for the case of EOS I, where it can even underestimate the Kepler limit for $\mathcal{R} < 0$. We see that in the fixed central-density sequences considered here, the local maximum of the Kepler rate is always attained for the co-rotating configuration (i.e. $\mathcal{R} = 0$), which contrasts with the case of fixed-mass sequences as considered in the Newtonian study [10]. A similar feature of the Kepler-rate decreasing as $\mathcal{R}$ decreases through zero can be seen in the mean-field results of Comer [12].

In the Fig. 6, we show the fluid surfaces of the two fluids rotating at the Kepler-rate for two different relative rotation rates, $\mathcal{R} = 0.1$ and $\mathcal{R} = 0.01$ respectively. We see the characteristic "cusp" appearing at the equator of the outer fluid, which indicates the onset of mass-shedding if the rotation rate were to be increased any further. Because we fixed the central densities of these configurations to those of the static case, it can be seen from Fig. 7 that both of these configurations belong to the so-called "supramassive" class, i.e. they do not have a corresponding stable non-rotating configuration of equal baryon-mass.

Fig. 7 shows the mass-density diagram for the static configuration of EOS I and for three Kepler configurations with different relative rotation-rates. The configurations to the right of the maximum are on the so-called "unstable branch", because they will be subject to unstable modes under small perturbations. The configurations above the dotted line correspond to stars on the unstable-branch of the static curve. They have no stable non-rotating counter-part, even if they are on the stable branch of the mass-curve of the rotating case, and they are therefore called "supramassive stars". These configurations are stabilized by rotation and would become unstable if slowed down below a critical rotation rate.

So far we have considered stars chemical equilibrium at the center, i.e. $\mu_n = \mu_p$. Incidentally, for the EOS-class considered here, the resulting static configurations share a common outer surface in this case. However, global chemical equilibrium is generally not possible for configurations with the two fluids rotating at different rates, which was shown by Andersson and Comer [9] and Prix

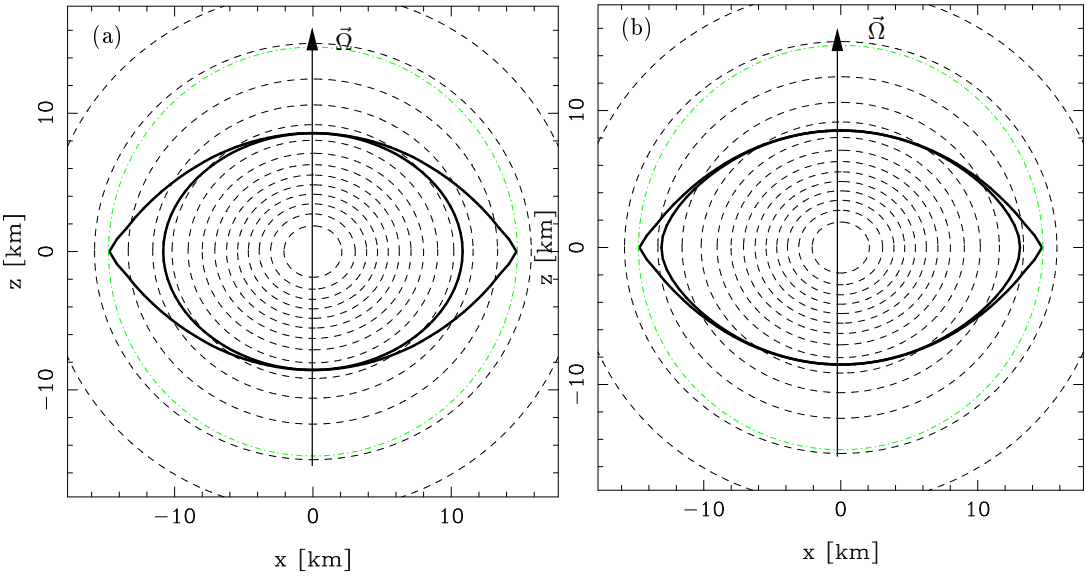

FIG. 6: Kepler configurations for EOS I. In figure (a) the relative rotation rate is $\mathcal{R} = 0.1$, while in (b) it is $\mathcal{R} = 0.01$.

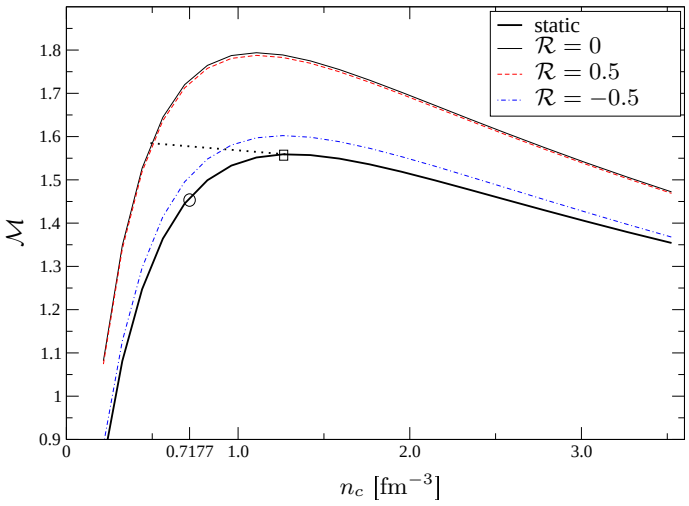

FIG. 7: Gravitational mass $\mathcal{M}$ as a function of central baryon number density n_c for EOS I with fixed central proton fraction of $x_\mathrm{p} = 0.05$. The four curves correspond to the non-rotating case, the co-rotating Kepler-configuration ($\mathcal{R} = 0$), and two Kepler-configurations with relative rotation rates of $\mathcal{R} = 0.5$ and $\mathcal{R} = -0.5$ respectively. The circle indicates a static configuration with central chemical potentials of $\mu_\mathrm{n} = \mu_\mathrm{p} = 0.3\ m_b c^2$. The box indicates the maximum-mass configuration in the static case. The dotted line represents the sequence of constant baryon mass connecting to the static maximum-mass configuration. Configurations above this line have no stable non-rotating counterpart and are called "supramassive" stars.

et al. [10]. In order to model more "realistic" configurations, in which the proton-fluid mimics a neutron-star "crust" (albeit without any solidity) by extending further outside than the neutrons, we can easily achieve this by choosing different central chemical potentials. For example, using EOS II and setting $\mu_\mathrm{n} = 0.228\ m_b c^2$ and $\mu_\mathrm{p} = 0.220\ m_b c^2$, we obtain the configuration shown in Fig. 8. For this figure we have chosen the rotation rate of the fastest known millisecond pulsar, which has a period of $P \sim 1.56$ ms.

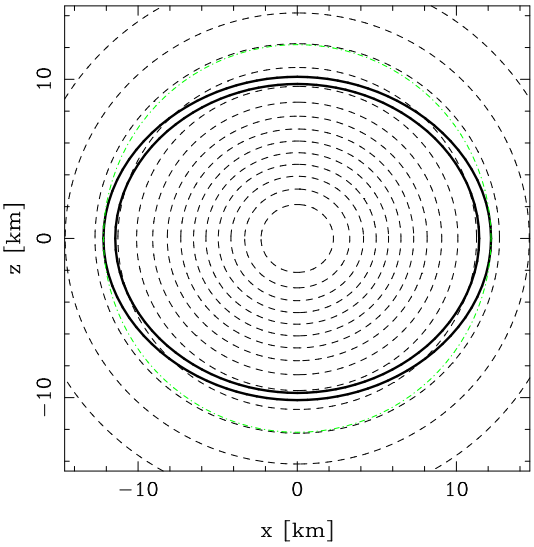

FIG. 8: Configuration with protons rotating at the speed of the fastest known millisecond pulsar, $\Omega_\mathrm{p}/2\pi = 641$ Hz, and $\Omega_\mathrm{n}/2\pi = 645$ Hz. The protons are extending further outside than the neutrons. The physical parameters are $\mu_\mathrm{n} = 0.228\ m_b c^2$ and $\mu_\mathrm{p} = 0.220\ m_b c^2$, resulting in central baryon number density $n_c = 0.561$ fm^{-3}, proton fraction $x_\mathrm{p} = 0.09$ and a gravitational mass of $\mathcal{M} = 1.39\ M_\odot$.

A similar configuration with $\mu_\mathrm{n} = 0.28\ m_b c^2$ and $\mu_\mathrm{p} = 0.3\ m_b c^2$ rotating at the Kepler-limit for a relative rotation rate of $\mathcal{R} = 0.01$ is displayed in Fig. 9. As can be seen by the cusp-formation, the Kepler-limit is

determined by the *outer* fluid, i.e. the protons in this case, despite the fact that they are rotating *more slowly* than the neutrons. This contrasts with the case depicted in Fig. 5, in which the faster fluid also happens to be the outer fluid, which is a particularity of this EOS-class and the choice of central chemical equilibrium $\mu_{\rm n} = \mu_{\rm p}$ (cf. [10]).

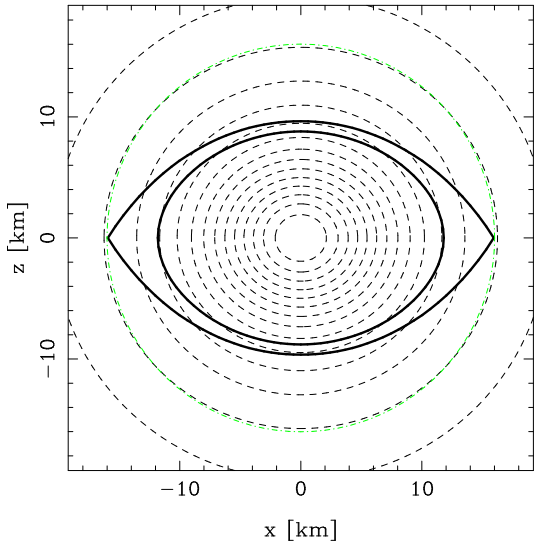

FIG. 9: Kepler configuration with $\mathcal{R} = 0.01$, $\mu_{\rm n} = 0.28\ m_b c^2$ and $\mu_{\rm p} = 0.3\ m_b c^2$, corresponding to a central baryon number density of $n_c = 0.716$ fm^{-3}, proton fraction $x_{\rm p} = 0.09$ and a gravitational mass of $\mathcal{M} = 1.57\ M_\odot$. The protons extend to the outer surface. The maximal rotation rates are found as $\Omega_{\rm n}/2\pi = 924.5$ Hz and $\Omega_{\rm p}/2\pi = 915.3$ Hz.

VII. CONCLUSIONS

We have developed a theoretical framework and a numerical code for computing stationary, fully relativistic superfluid neutron star models.

Using this code we have reconfirmed the existence of oblate-prolate shaped two-fluid configurations, previously shown in [10, 14]. We have studied the dependency of the Kepler rate of a two-fluid star on the relative rotation rate $\mathcal{R}$. We have compared this to the Kepler-rate predicted by a Newtonian slow-rotation approximation, which is found to typically overestimate the Kepler-rate by about 15%, but which can also sometimes underestimate it, as seen in the case of EOS I and $\mathcal{R} \lesssim -0.25$ (cf. Fig. 5).

The relative rotation rate can also have a large influence (at fixed central density) on the mass-density relation, as shown in Fig. 7.

Another interesting aspect of this model is that we are not restricted to configurations in chemical equilibrium at the center. Choosing the central chemical potentials to be different allows one to emulate a neutron star "crust" (albeit a fluid one), as one fluid will now extend further outwards than the other, as seen in Fig. 8 and Fig. 9. One interesting observation from such configurations is that the Kepler-limit will be determined by the outer fluid (forming a cusp), while this can actually be rotating *slower* then the inner fluid.

We currently use a (quite general) EOS class of two-fluid polytropes, but this can be extended straightforwardly to more "realistic" nuclear-physics equations of state. In particular it might be interesting in the next step to use the first relativistic two-fluid EOS incorporating entrainment by Comer and Joynt [13]. Furthermore it would be important to add the presence of a solid crust and to allow for differential rotation in the superfluid neutrons (differential rotation in single-fluid stars has been implemented and used in LORENE already, cf. [29, 30]).

The astrophysically most interesting future extension of this work would probably consist in studying the oscillation modes of such models, which would be directly related to the emission of gravitational waves. In these non-stationary situations, however, dissipative mechanisms like viscosity and mutual friction would also start to play a role and should be included in the model.

APPENDIX A: THE NEWTONIAN ANALYTIC SLOW-ROTATION SOLUTION

A method for solving the stationary 2-fluid configuration in the Newtonian slow-rotation approximation was initially developed in [8], and was completed to include all EOS-interactions in [10] (in the following referred to as Paper I). Using this method, an analytic solution was found in Paper I for equations of state of the form $\mathcal{E} = \frac{1}{2}\kappa_{\rm n} n_{\rm n}^2 + \frac{1}{2}\kappa_{\rm p} n_{\rm p}^2 + \kappa_{\rm np} n_{\rm n} n_{\rm p} + \beta^{\rm p} n_{\rm p} \Delta^2$. While this solution was very useful for studying the qualitative properties of an interacting 2-fluid system, it is unfortunately not very suitable for comparison to the numerical solution presented in this paper. The reason for this lies in the somewhat unphysical behavior of entrainment in this model. Namely, the entrainment numbers (16) are found as $\varepsilon_{\rm p} = 2\beta^{\rm p}/m$, and $\varepsilon_{\rm n} = 2x_{\rm p}\beta^{\rm p}/(m(1-x_{\rm p}))$, where $x_{\rm p} \equiv n_{\rm p}/n$ is the proton fraction, which is constant for this EOS (cf. Paper I). Therefore the entrainment numbers are constant, independently of the densities, and so the entrainment effect would still be present in a 1-fluid region. This unphysical behavior does not pose a problem in the slow-rotation approximation, which consists of an expansion around a static chemical-equilibrium configuration: the two fluids share a common surface in the unperturbed state, and the rotation will only induce infinitesimal displacements of the fluids. In this framework there are therefore no finite 1-fluid regions. However, in a numerical code allowing for arbitrary rotations and deviations from chemical equilibrium, such an entrainment model would be problematic. The EOS-class (68) used in this work is therefore preferable on both physical and numerical grounds.

Fortunately, an analytic solution can also be found for

this physically preferable EOS using the slow-rotation approach developed in Paper I. This solution is very valuable for quantitative comparisons with our numerical results presented in section V C. Here we derive this new analytic solution, skipping some of the more technical steps, which have been explained in more detail already in Paper I.

Because of axisymmetry, the rotating solution only depends on the spherical coordinates r and θ, while the static configuration is assumed to be spherically symmetric. The 2-fluid slow-rotation approximation proceeds by expanding any local stellar quantity Q as follows:

$$Q(r,\theta;\Omega_X) = Q^{(0)}(r) + \Omega_X\, Q^{XY}(r,\theta)\,\Omega_Y + \mathcal{O}(\Omega^4)\,, \quad \text{(A1)}$$

where here and in the following we automatically sum over repeated constituent indices $X = \mathrm{n,p}$. We can separate the variables r and θ by expanding in Legendre Polynomials, i.e. $Q^{XY}(r,\theta) = \sum_l Q^{XY}_l(r) P_l(\cos\theta)$, and it can be shown that only the components $l = 0, 2$ will be nonzero in the solution. The solution is therefore fully determined by two ordinary differential equations for the components $\Phi^{XY}_0(r)$ and $\Phi^{XY}_2(r)$ of the perturbation of the gravitational potential. The information about the EOS enters via the following two "structure functions", defined as

$$\mathcal{S}_{XY} \equiv \left(\left.\frac{\partial^2 \mathcal{E}}{\partial n_X \partial n_Y}\right|_0 \right)^{-1}, \quad \beta^X \equiv \left.\frac{\partial^2 \mathcal{E}}{\partial n_X \partial \Delta^2}\right|_0, \quad \text{(A2)}$$

where $|_0$ denotes the derivatives to be evaluated at the static configuration. For the EOS (68), we find

$$\mathcal{S}_{XY} = \frac{1}{\mathcal{K}} \begin{pmatrix} \kappa_\mathrm{p} & -\kappa_\mathrm{np} \\ -\kappa_\mathrm{np} & \kappa_\mathrm{n} \end{pmatrix}, \quad \text{(A3)}$$

where $\mathcal{K} \equiv \kappa_\mathrm{p}\kappa_\mathrm{n} - \kappa^2_\mathrm{np}$, and

$$\beta^X(r) = \kappa_\Delta M^{XY} n^{(0)}_Y(r)\,, \quad \text{(A4)}$$

with the constant matrix M^{XY} defined as

$$M^{XY} \equiv \begin{pmatrix} 0 & 1 \\ 1 & 0 \end{pmatrix}. \quad \text{(A5)}$$

We further introduce the "derived" structure functions,

$$k_A \equiv \mathcal{S}_{AB} m^B\,, \quad \text{and} \quad k \equiv m^A k_A\,, \quad \text{(A6)}$$

which are constant for this EOS. The matrices E^{XY}_A, defined as

$$E^{XY}_A(r) \equiv \frac{1}{3}\mathcal{S}_{AB}\left(\delta^{B,XY} - 2\beta^B(r)\,\Delta^{XY}\right), \quad \text{(A7)}$$

are now functions of r, contrary to the EOS treated in Paper I, in which they were constant. The constant auxiliary matrices $\delta^{A,XY}$ and Δ^{XY} are defined as

$$\delta^{\mathrm{n},XY} \equiv \begin{pmatrix} m^\mathrm{n} & 0 \\ 0 & 0 \end{pmatrix}, \quad \delta^{\mathrm{p},XY} \equiv \begin{pmatrix} 0 & 0 \\ 0 & m^\mathrm{p} \end{pmatrix}, \quad \text{(A8)}$$

$$\Delta^{XY} \equiv \begin{pmatrix} 1 & -1 \\ -1 & 1 \end{pmatrix}. \quad \text{(A9)}$$

The *static* background solution only depends on $\mathcal{S}_{XY}$, and is identical to the one found in Paper I. Namely, in "natural units" defined by $\rho^{(0)}(0) = 1$ and $R = 1$, this static solution can be written as

$$\rho^{(0)}(r) = \frac{\sin(r\sqrt{k})}{r\sqrt{k}}. \quad \text{(A10)}$$

In these units it must be true that $\rho^{(0)}(1) = 0$, which leads to the condition $k = m^A k_A = \pi^2$. This relation can be used to rescale the EOS parameters κ_n, κ_p and κ_np to natural units. The respective particle number densities $n^{(0)}_A(r)$ are expressible as

$$n^{(0)}_A(r) = \frac{k_A}{\pi^2}\rho^{(0)}(r)\,. \quad \text{(A11)}$$

Substituting this into (A7), we can write

$$E^{XY}_A(r) = \widetilde{E}^{XY}_A - \hat{E}^{XY}_A \rho^{(0)}(r)\,, \quad \text{(A12)}$$

in terms of the two constant matrices

$$\begin{aligned} \widetilde{E}^{XY}_A &\equiv \frac{1}{3}\mathcal{S}_{AB}\delta^{B,XY}\,, \\ \hat{E}^{XY}_A &\equiv \frac{2}{3\rho^{(0)}}\,\mathcal{S}_{AB}\beta^B\,\Delta^{XY}\,, \end{aligned} \quad \text{(A13)}$$

and for $E^{XY} \equiv m^A E^{XY}_A$, we write in an analogous manner

$$E^{XY} = \widetilde{E}^{XY} - \hat{E}^{XY}\,\rho^{(0)}(r)\,, \quad \text{(A14)}$$

with

$$\begin{aligned} \widetilde{E}^{XY} &= \frac{1}{3}k_B\delta^{B,XY}\,, \\ \hat{E}^{XY} &= \frac{4\kappa_\Delta}{3\pi^2}\,k_\mathrm{n}k_\mathrm{p}\,\Delta^{XY}\,. \end{aligned} \quad \text{(A15)}$$

We can now write the differential equations determining the solution for the given EOS, namely

$$\mathcal{D}_0\Phi^{XY}_0 + \pi^2\,\Phi^{XY}_0 = \mathcal{C}^{XY} + r^2\widetilde{E}^{XY} - r^2\rho^{(0)}\hat{E}^{XY}, \quad \text{(A16)}$$

$$\mathcal{D}_2\Phi^{XY}_2 + \pi^2\,\Phi^{XY}_2 = -r^2\widetilde{E}^{XY} + r^2\rho^{(0)}\hat{E}^{XY}, \quad \text{(A17)}$$

where the differential operator $\mathcal{D}_l$ is defined as

$$\mathcal{D}_l \equiv \frac{d^2}{dr^2} + \frac{2}{r}\frac{d}{dr} - \frac{l(l+1)}{r^2}\,. \quad \text{(A18)}$$

We note that the only difference of this EOS to the one studied in Paper I concerns the entrainment $\beta^X(r)$. We can therefore formally recover the results from Paper I in the limit $\kappa_\Delta \to 0$, which corresponds to $\hat{E}^{XY} \to 0$ and $\hat{E}^{XY}_A \to 0$. The constant matrix $\mathcal{C}^{XY}$ is determined by the choice of stellar sequence, e.g. either characterized by fixed central densities (FCD) or fixed masses (FM). The solution to the above equations also determines the density distribution of the two-fluid star, namely via the relations

$$n^{XY}_{A,0}(r) = \mathcal{S}_{AB}\,\mathcal{C}^{B,XY} + r^2 E^{XY}_A - k_A\Phi^{XY}_0\,, \quad \text{(A19)}$$

$$n^{XY}_{A,2}(r) = -r^2 E^{XY}_A - k_A\Phi^{XY}_2\,, \quad \text{(A20)}$$

where the constants $\mathcal{C}^{A,XY}$ are also determined by the choice of stellar sequence, and they satisfy the relation $\mathcal{C}^{XY} = k_A \mathcal{C}^{A,XY}$. The complete slow-rotation solution for the density distribution of the two fluids can be written as

$$n_A(r,\theta) = n_A^{(0)}(r) + \Omega_X \left(n_{A,0}^{XY} + n_{A,2}^{XY} P_2(\cos\theta) \right) \Omega_Y \,. \tag{A21}$$

The general (regular) solution of equations (A16) and (A17) can be found explicitly as

$$\begin{aligned} \Phi_0^{XY}(r) &= \mathcal{A}_0^{XY} \frac{J_{1/2}(r\pi)}{\sqrt{r}} + \frac{\widetilde{E}^{XY}}{\pi^2}\left(r^2 - \frac{6}{\pi^2}\right) + \frac{\mathcal{C}^{XY}}{\pi^2} \\ &\quad - \frac{\hat{E}^{XY}}{12\pi^4}\left\{3r\pi \sin r\pi + (3 - 2\pi^2 r^2)\cos r\pi\right\} \,, \end{aligned} \tag{A22}$$

$$\begin{aligned} \Phi_2^{XY}(r) &= \mathcal{A}_2^{XY} \frac{J_{5/2}(r\pi)}{\sqrt{r}} - \frac{\widetilde{E}^{XY}}{\pi^2} r^2 \\ &\quad - \frac{\hat{E}^{XY}}{12\pi^7 r^3}\left\{(45 + 2\pi^4 r^4)\, r\pi \, \cos r\pi \right. \\ &\qquad \left. + 15(r^2\pi^2 - 3)\, \sin r\pi\right\} \,, \end{aligned} \tag{A23}$$

where $\mathcal{A}_0^{XY}$ and $\mathcal{A}_2^{XY}$ are constants of integration, and $J_n(x)$ are the standard Bessel functions. One can verify the asymptotic behavior $\Phi_2^{XY} \sim r^2$ as $r \to 0$, which is required for regularity. In addition to the regularity requirements at the center, the solution must satisfy the following boundary condition at the surface ($r = 1$):

$$\Phi_l^{XY\prime}(1) + l(l+1)\Phi_l^{XY}(1) = 0 \,. \tag{A24}$$

These boundary conditions result in the following relations for the integration constants A_0^{XY} and A_2^{XY}:

$$\begin{aligned} 4\pi^4\sqrt{2}\,\mathcal{A}_0^{XY} &= 12(\pi^2 - 2)\widetilde{E}^{XY} + (1 - \pi^2)\hat{E}^{XY} \\ &\quad + 4\pi^2 \mathcal{C}^{XY} \,, \end{aligned} \tag{A25}$$

$$\sqrt{2}\,\mathcal{A}_2^{XY} = \frac{5}{\pi^2}\widetilde{E}^{XY} - \frac{5}{12\pi^4}(3 + 2\pi^2)\hat{E}^{XY}. \tag{A26}$$

Fixed central density (FCD) sequence

The FCD-sequence is the most directly comparable to the numerical results discussed in this paper. This sequence is defined by the condition $n_{A,0}^{XY}(0) = 0$, and in this case the remaining constant of integration can be determined as

$$\mathcal{C}_{\rm FCD}^{XY} = -3\left(1 - \frac{4}{\pi^2}\right)\widetilde{E}^{XY} + \frac{1}{4}\hat{E}^{XY} \,, \tag{A27}$$

and we also have the relation

$$\mathcal{S}_{AB}\mathcal{C}_{\rm FCD}^{B,XY} = \frac{k_A}{\pi^2}\,\mathcal{C}_{\rm FCD}^{XY} \,. \tag{A28}$$

Putting all the pieces together, we arrive at the following explicit solution for the density perturbations of the FCD sequence:

$$\begin{aligned} n_{A,0,\rm FCD}^{XY} &= -\frac{6k_A\widetilde{E}^{XY}}{\pi^4}\left(\frac{\sin r\pi}{r\pi} + \frac{r^2\pi^2}{6} - 1\right) + \widetilde{E}_A^{XY} r^2 \\ &\quad - \frac{k_A\hat{E}^{XY}}{4\pi^4}\left((1 - r^2\pi^2)\frac{\sin r\pi}{r\pi} - (1 - \frac{2}{3}r^2\pi^2)\cos r\pi\right) \\ &\quad - \frac{\hat{E}_A^{XY}}{\pi^2} r\pi \sin r\pi \,, \end{aligned} \tag{A29}$$

$$\begin{aligned} n_{A,2}^{XY}(r) &= \frac{k_A\widetilde{E}^{XY}}{\pi^2}\left(r^2 - \frac{5}{\sqrt{2}}\frac{J_{5/2}(r\pi)}{\sqrt{r}}\right) - \widetilde{E}_A^{XY}\, r^2 \\ &\quad + \frac{5}{6}\frac{k_A\hat{E}^{XY}}{\pi^5 r^3}\left\{\left(\frac{\pi^2}{5}r^4 - 3\right) r\pi\cos r\pi - (r^2\pi^2 - 3)\sin r\pi\right\} \\ &\quad + \frac{\hat{E}_A^{XY}}{\pi^2}\, r\pi \sin r\pi \,, \end{aligned} \tag{A30}$$

in terms of the constant "structure matrices" $\widetilde{E}$ and $\hat{E}$ defined in Eqs. (A13) and (A15).

Fixed-mass (FM) stellar sequence

For completeness we also give the solution corresponding to a fixed-mass sequence, which might even be physically more interesting. The difference to the FCD-solution only concerns the $l = 0$ component, while $n_{A,2}^{XY}$ is the same in both cases. As discussed in Paper I, the FM-sequence is characterized by the conditions

$$\int_0^1 r^2\, n_{A,0,\rm FM}^{XY}(r)\, dr = 0 \,, \tag{A31}$$

which lead to the following condition for the potential

$$\Phi_{0,\rm FM}^{XY}(1) = 0 \,. \tag{A32}$$

This results in the integration constant

$$\mathcal{C}_{\rm FM}^{XY} = \left(\frac{6}{\pi^2} - 1\right)\widetilde{E}^{XY} + \left(\frac{1}{6} - \frac{1}{4\pi^2}\right)\widetilde{E}^{XY} \,, \tag{A33}$$

while we can similarly determine $\mathcal{S}_{AB}\mathcal{C}^{B,XY}$ from (A31). Inserting this into (A22) we get

$$\begin{aligned} \Phi_{0,\rm FM}^{XY}(r) &= \frac{\widetilde{E}^{XY}}{\pi^2}\left(r^2 - 1 + \sqrt{2}\frac{J_{1/2}(r\pi)}{\sqrt{r}}\right) \\ &\quad + \frac{\hat{E}^{XY}}{12\pi^4}\left(2\pi^2 - 3 + (2\pi^2 r^2 - 3)\cos r\pi \right. \\ &\qquad \left. - (1 + 3r^2)\frac{\pi^2}{\sqrt{2}}\frac{J_{1/2}(r\pi)}{\sqrt{r}}\right) . \end{aligned} \tag{A34}$$

The $l = 0$ density coefficient is therefore found by using (A19):

$$n_{A,0,\rm FM}^{XY} = \frac{k_A\widetilde{E}^{XY}}{5\pi^4}\left(30 + 3\pi^2 - 5r^2\pi^2 - \frac{10\pi}{r}\sin r\pi\right)$$

$$+\widetilde{E}_A^{XY}\left(r^2-\frac{3}{5}\right)+\frac{\hat{E}_A^{XY}}{\pi^2}\left(3(1-\frac{6}{\pi^2})-r\pi\sin r\pi\right)$$
$$-\frac{k_A\hat{E}^{XY}}{12\pi^4}\left(36(1-\frac{6}{\pi^2})-(3-2r^2\pi^2)\cos r\pi\right.$$
$$\left.-(1+3r^2)\frac{\pi}{r}\sin r\pi\right)\,, \qquad \text{(A35)}$$

which completes the analytic solution in the FM case.

Calculating the Kepler-limit

We briefly review the method of calculating the Kepler-limit using the slow-rotation solution presented above. The result of this calculation was used for the Newtonian slow-rotation Kepler-limit presented in Fig. 5. As derived in Paper I, the Kepler-rate to order Ω^2 for each of the two fluids can be expressed as the solution of the equation

$$\Omega_A^2=\Omega_{(0)}^2+\Omega_X\,\delta q_A^{XY}\,\Omega_Y+\mathcal{O}(\Omega^4)\,, \qquad \text{(A36)}$$

where the zeroth-order expression is

$$\Omega_{(0)}^2=\Phi^{(0)'}(1)\,, \qquad \text{(A37)}$$

and the second-order correction terms reads as

$$\delta q_A^{XY}=\left[-\frac{3}{k_A}\left(n_{A,0}^{XY}-\frac{1}{2}n_{A,2}^{XY}\right)+\Phi_0^{XY'}-\frac{1}{2}\Phi_2^{XY'}\right]_{r=1}. \qquad \text{(A38)}$$

For the EOS-class considered here, we find

$$\Omega_{(0)}^2 \;=\; \frac{4}{\pi}G\,\rho(0)\,, \qquad \text{(A39)}$$

$$\delta q_{A,\mathrm{FCD}}^{XY} \;=\; -\frac{9\widetilde{E}_A^{XY}}{2k_A}+\frac{\hat{E}^{XY}}{12\pi^4}\left(6-7\pi^2\right)$$
$$+\frac{\hat{E}^{XY}}{\pi^4}\left(5\pi^2-24\right)\,, \qquad \text{(A40)}$$

$$\delta q_{A,\mathrm{FM}}^{XY} \;=\; \frac{6}{\pi^2}\left(\frac{1}{5}-\frac{3}{\pi^2}\right)\widetilde{E}^{XY}-\frac{9\hat{E}_A^{XY}}{k_A\pi^4}(\pi^2-6)$$
$$-\frac{\hat{E}^{XY}}{4\pi^6}\left(216-39\pi^2+2\pi^4\right)-\frac{27}{10k_A}\widetilde{E}_A^{XY}\,. \qquad \text{(A41)}$$

For each fluid A, we find the Kepler-limit $\Omega_{\mathrm{K}A}(\Omega_B)$ (where $B\neq A$) by solving the quadratic equation (A36). The Kepler-limit is then interpreted as the corresponding solution for the *faster* fluid, which in this case corresponds to the outer fluid, i.e. we have

$$\Omega_{\mathrm{K}}=\begin{cases}\Omega_{\mathrm{K,n}}(\mathcal{R})\,, & \text{for}\quad \mathcal{R}>0\,,\\ \Omega_{\mathrm{K,p}}(\mathcal{R})\,, & \text{for}\quad \mathcal{R}<0\,.\end{cases} \qquad \text{(A42)}$$

ACKNOWLEDGMENTS

RP acknowledges support from the EU Programme 'Improving the Human Research Potential and the Socio-Economic Knowledge Base' (Research Training Network Contract HPRN-CT-2000-00137). GC acknowledges support from NSF grant PHYS-0140138.

[1] B. Abbot et al. (LIGO Scientific Collaboration), Phys. Rev. D. **69**, 082004 (2004).
[2] M. Baldo, J. Cugnon, A. Lejeune, and U. Lombardo, Nucl. Phys. A **536**, 349 (1992).
[3] O. Sjöberg, Nucl. Phys. A **265**, 511 (1976).
[4] B. Link, R. I. Epstein, and J. M. Lattimer, in *Stellar Astrophysics, Proceedings of the Pacific Rim Conference*, edited by L. Cheng, H. Chau, K. Chan, and K. Leung (Kluwer Academic Publishers, Netherlands, 2000), p. 117.
[5] B. Carter, D. Langlois, and D. M. Sedrakian, A&A **361**, 795 (2000).
[6] N. Andersson, G. L. Comer, and R. Prix, Phys. Rev. Lett. **90**, 091101 (2003).
[7] N. Andersson, G. L. Comer, and R. Prix, to appear in MNRAS (2004).
[8] R. Prix, A&A **352**, 623 (1999).
[9] N. Andersson and G. L. Comer, Class. Quant. Grav. **18**, 969 (2001).
[10] R. Prix, G. L. Comer, and N. Andersson, A&A **381**, 178 (2002).
[11] S. Yoshida and Y. Eriguchi, MNRAS **347**, 575 (2004).
[12] G. L. Comer, Phys. Rev. D. **69**, 123009 (2004).
[13] G. L. Comer and R. Joynt, Phys. Rev. D. **68**, 023002 (2003).
[14] R. Prix, J. Novak, and G. L. Comer, in *Proceedings of the Spanish Relativist Meeting 2002. Gravitation and Cosmology.*, edited by A. Lobo (Universitat de Barcelona, 2002), pp. 212–217.
[15] B. Carter, in *Relativistic Fluid Dynamics (Noto, 1987)*, edited by A. Anile and M. Choquet-Bruhat (Springer-Verlag, Heidelberg, 1989), vol. 1385 of *Lecture Notes in Mathematics*, pp. 1–64.
[16] G. L. Comer and D. Langlois, Class. Quantum Grav. **11**, 709 (1994).
[17] B. Carter and D. Langlois, Nucl. Phys. **B531**, 478 (1998).
[18] D. Langlois, D. M. Sedrakian, and B. Carter, MNRAS **297**, 1189 (1998).
[19] B. Carter, in *A Random Walk in General Relativity and Cosmology*, edited by N. Dadhich, J. K. Rao, J. Narlikar, and C. Vishveshwara (Wiley Eastern, Bombay, 1983), pp. 49–62.
[20] B. Carter, Comm. Math. Phys. **17**, 233 (1970).
[21] E. Gourgoulhon, P. Haensel, R. Livine, E. Paluch, S. Bonazzola, and J.-A. Marck, A&A **349**, 851 (1999).
[22] L. Smarr and J. W. York, Phys. Rev. D. **17**, 2529 (1978).

[23] S. Bonazzola, E. Gourgoulhon, M. Salgado, and J.-A. Marck, A&A **278**, 421 (1993).
[24] E. Gourgoulhon and S. Bonazzola, Class. Quant. Grav. **11**, 443 (1994).
[25] S. Bonazzola and E. Gourgoulhon, Class. Quant. Grav. **11**, 1175 (1994).
[26] *LORENE, a C++ library for numerical relativity. Published under the GPL licence.*, `http://www.lorene.obspm.fr`.
[27] R. Prix and M. Rieutord, A&A **393**, 949 (2002).
[28] N.-C. Chao, J. W. Clark, and C.-H. Yang, Nucl. Phys. A **179**, 320 (1972).
[29] L. Villain, J. A. Pons, P. Cerdá-Durán, and E. Gourgoulhon, A&A **418**, 283 (2004).
[30] J.-O. Goussard, P. Haensel, and J. L. Zdunik, A&A **330**, 1005 (1998).